Cosmic microwave background anisotropies in the timescape cosmology

M. Ahsan Nazer* and David L. Wiltshire†
Department of Physics & Astronomy, University of Canterbury, Private Bag 4800, Christchurch 8140, New Zealand

We analyze the spectrum of cosmic microwave background (CMB) anisotropies in the timescape cosmology: a potentially viable alternative to homogeneous isotropic cosmologies without dark energy. We exploit the fact that the timescape cosmology is extremely close to the standard cosmology at early epochs to adapt existing numerical codes to produce CMB anisotropy spectra, and to match these as closely as possible to the timescape expansion history. A variety of matching methods are studied and compared. We perform Markov chain Monte Carlo analyses on the parameter space, and fit CMB multipoles $50 \leq \ell \leq 2500$ to the Planck satellite data. Parameter fits include a dressed Hubble constant, $H_0 = 61.0\,\mathrm{km\ sec^{-1}\,Mpc^{-1}}$ ($\pm 1.3\%$ stat) ($\pm 8\%$ sys), and a present void volume fraction $f_{\mathrm{v}0} = 0.627$ ($\pm 2.3\%$ stat) ($\pm 13\%$ sys). We find best fit likelihoods which are comparable to that of the best fit ΛCDM cosmology in the same multipole range. In contrast to earlier results, the parameter constraints afforded by this analysis no longer admit the possibility of a solution to the primordial lithium abundance anomaly. This issue is related to a strong constraint between the ratio of baryonic to nonbaryonic dark matter and the ratio of heights of the second and third acoustic peaks, which cannot be changed as long as the standard cosmology is assumed up to the surface of last scattering. These conclusions may change if backreaction terms are also included in the radiation–dominated primordial plasma.

PACS numbers: 98.80.-k 98.80.Es 04.20.-q. *Physical Review D* **91**, 063519 (2015).

I. INTRODUCTION

The timescape cosmology [1–3] is a viable alternative to the standard cosmology, without dark energy. It abandons the assumption that average cosmic evolution is identical to that of an exactly homogeneous isotropic Friedmann–Lemaître–Robertson–Walker (FLRW) model, but relies on a simplifying principle concerning gravitational energy and average cosmic evolution [4] to obtain a phenomenologically predictive model [3, 5–8].

The assumption of spatial homogeneity is observationally well justified at the epoch of last scattering, given the evidence of the cosmic microwave background (CMB) radiation. However, eventually the growth of structure becomes nonlinear with respect to perturbation theory about a FLRW model, and by the present epoch the Universe is only homogeneous in some average statistical sense when one averages on scales $\gtrsim 100\,h^{-1}$Mpc, where h is the dimensionless parameter related to the Hubble constant by $H_0 = 100h\,\mathrm{km\ sec^{-1}\,Mpc^{-1}}$.

The exact spatial scale of the transition to average homogeneity, which we will call the statistical homogeneity scale, is debated [9–11]. However, the most conservative estimates are that it occurs in the range 70–$100\,h^{-1}$Mpc [11]. This is consistent with the idea adopted in the timescape scenario that it is the small amplifications of initial perturbations by acoustic waves in the primordial plasma on scales smaller than the $\sim 100\,h^{-1}$Mpc baryon acoustic oscillation scale which determine the transition to the nonlinear regime [12]. Below the statistical homogeneity scale we observe a universe dominated in volume by voids [13–15], with clusters of galaxies in walls, sheets and filaments surrounding and threading the voids. Voids of diameter $\sim 30\,h^{-1}$Mpc form some 40% of the volume of the present epoch Universe [13, 14]. They represent the largest typical structures, though there are some larger less typical structures [15–17], and also a numerous population of smaller minivoids [18].

The problem of fitting a smooth geometry [19, 20] to the complex hierarchy of the observed cosmic web requires addressing a number of fundamental questions [21], including: (i) how is average cosmic evolution to be described; and (ii) how are local observables related to quantities defined with respect to some average geometry? The fitting problem is not directly addressed in the standard cosmology. One simply assumes that average evolution follows a FLRW model. However, FLRW models expand rigidly to maintain constant spatial curvature, a feature which is not generic in general relativity and which is absent even in simple inhomogeneous models such as the Lemaître–Tolman–Bondi (LTB) [22–24] and Szekeres [25] solutions.

General inhomogeneous cosmological models which begin close to a spatially homogeneous isotropic model will exhibit backreaction (see, e.g, [26–28]), leading to a non-FLRW expansion. However, the general situation is so complex that even when studying inhomogeneity and backreaction, many researchers simply assume an average FLRW expansion, given the phenomenological success of the standard model. If "dark energy" is to have a deep physical explanation, however, then the phenomenological success of the standard model should be taken as a

*Electronic address: Ahsan.Nazer@pg.canterbury.ac.nz
†Electronic address: David.Wiltshire@canterbury.ac.nz

signal that there are simplifying principles to be found in the averaging problem. The timescape model relies on such a simplification [4]: there is always a choice of clocks and rulers of canonical observers which makes the average Hubble expansion uniform despite inhomogeneity.

To a achieve a notion of average uniform but nonrigid expansion one gives up the assumption that in the presence of spatial curvature gradients the clocks of all average observers are synchronized. It is well understood that observers at fixed spatial coordinates in a standard perturbed FLRW universe with geometry,

$$\mathrm{d}s^2 = -(1+2\Phi)c^2\mathrm{d}t^2 + a^2(1-2\Psi)\delta_{ij}\mathrm{d}x^i\mathrm{d}x^j, \qquad (1)$$

in Newtonian gauge, will have clock rates that differ slightly from cosmic time, t, on account of their position in the gravitational potential $\Phi(t,\mathbf{x})$. However, although all actual observers exist in bound structures deep within the nonlinear regime of perturbation theory, a time dilation effect of the magnitude in the timescape model has previously been overlooked due to a prejudice that there can be no significant time dilation for weak fields. Such physical intuition is driven by our experience of strong field gravity for isolated systems, in which there is a well-defined canonical clock at spatial infinity. However, there are no isolated systems in the actual Universe, and the problem of calibrating the effective asymptotic clocks in regions of different densities in the absence of a timelike Killing vector is a qualitatively new one.

In the timescape scenario the relative volume deceleration of regions of different density is treated as a physical parameter in the normalization of average asymptotic clocks. Although the relative deceleration is instantaneously tiny (typically $\lesssim 10^{-10}\mathrm{m\ s}^{-2}$ [4]) and well within the weak field regime, when integrated over the lifetime of the Universe this can cumulatively lead to present epoch clock rate differences of order 35%. In particular, the present Universe is void–dominated whereas structure formation ensures that all actual observers, and objects which can be observed, are in regions of greater than critical density, giving us a mass–biased view of the Universe. There is a difference of calibration of the canonical clocks of comoving observers in volume–average environments (in voids) where there is no detectable matter relative to clocks in bound systems, which can be observed. Cosmic acceleration turns out to be an apparent effect, due to both: (i) the backreaction of inhomogeneities in changing the average evolution from a FLRW model; and (ii) the relation of the time parameter which best describes statistically average cosmic evolution to the physical clocks of observers in bound systems [1]. The cosmic coincidence problem is readily solved since apparent cosmic acceleration begins when the void volume fraction, $f_{\rm v}$, reaches a particular value $\sim 59\%$ [1].

After a variety of observational tests [5–8] the timescape model remains a viable alternative to the standard model. On large scales its expansion history is so close to that of the standard model that differences in luminosity distances are at the level of current systematic uncertainties in type Ia supernova data [6]; which model fits better depends on the method by which supernova light curves are reduced. On small scales, a study motivated by the timescape model has led to the discovery that the spherically averaged expansion of the Universe below the scale of statistical homogeneity is significantly more uniform in the rest frame of the Local Group of galaxies than in the standard CMB rest frame [29], a result which is very difficult to reconcile with the standard model.

To fully compete, observational tests of the timescape scenario need to be developed to a similar extent to the standard cosmology. One particularly important test is the detailed fitting of the acoustic peaks in the CMB anisotropy spectrum. Thus far we have successfully fit the angular diameter distance of the sound horizon at decoupling, which controls the overall angular scale of the acoustic peaks, thereby constraining cosmological parameters [5, 8]. However, a fit of the ratios of the peak heights has not yet been performed. This paper will remedy that situation: we will perform the first detailed fits of the acoustic peaks in the timescape scenario.

The problem is a very nontrivial one, since the timescape model revisits many of the foundational questions of cosmology from first principles, and much has to be rebuilt from scratch. The timescape scenario is based on a particular physical interpretation of the Buchert averaging formalism [30], and ideally in considering the early radiation dominated universe we should begin with the version of the formalism that directly includes the effects of pressure in the averaging procedure [31].

A from–first–principles investigation of the Buchert formalism in the radiation–dominated epoch using the constraining principles of the timescape scenario is a huge challenge, however. Thus we will adopt the same simplification that was made in our recent paper [8], in which we assume a standard perturbed FLRW evolution at early epochs which is smoothly matched to a matter plus radiation solution in which the effects of backreaction from the radiation fluid are neglected in determining background average cosmic evolution. Only the density gradients of nonrelativistic matter (both baryonic and nonbaryonic) are assumed to contribute to cosmic backreaction.

Such an approximation is justified by the fact that the Universe was definitely close to being homogeneous and isotropic at early times. This approximation also allows us to make use of standard CMB codes, to the extent that all quantities must be calibrated to late epoch evolution from the timescape model, which in itself requires considerable recoding, as will be described.

The plan of this paper is as follows: in Sec. II we briefly review the key features of the standard CMB acoustic peak analysis in the FLRW and LTB models. In Sec. III we extend this methodology to the timescape cosmology. In Sec. IV our numerical computation strategy is discussed. In Sec. V we present our key results of fitting the timescape cosmology to the CMB acoustic peaks with the Planck satellite data. Section VI contains a concluding

discussion.

II. CMB ANISOTROPY OVERVIEW

A. The standard FLRW model

The standard FLRW models are phenomenologically highly successful, and much of this success is built on their application to the problem of the evolution of perturbations in the early Universe, and the observable signatures of these perturbations as temperature fluctuations of order $\Delta T/T \sim 10^{-5}$ in the mean CMB temperature, $T = 2.7255\,\mathrm{K}$. The tools that have been developed for the analysis of CMB anisotropies, and the theoretical framework on which they are based, have taken decades of development. Since we assume that the standard approach is a good approximation at early times, we will adopt standard tools where possible. It is therefore useful to firstly recall the key features of the standard approach, in order to describe which features will remain unchanged and which will be revisited.

In the standard approach CMB anisotropies are determined from density fluctuations in the early Universe, which are calculated numerically by tracing the time evolution of the distributions of baryons, nonbaryonic Cold Dark Matter (CDM) and photons. The starting point is Boltzmann's equation

$$\hat{L}[f] = C[f] \tag{2}$$

for the time evolution of each particle distribution function, f, where $\hat{L}$ is the relativistic Liouville operator on the particle's phase space and C is a collision term describing particle production and destruction. The total time rate of change can be evaluated along the particle geodesics of a FLRW geometry with first order perturbations, such as (1) in the case of the Newtonian gauge. The Einstein field equations couple the distributions of all the interacting constituents into a system of differential equations generally referred to as the Einstein-Boltzmann equations. The presence of the collision term means that particle numbers are not necessarily conserved in phase space.

The principal epochs that are of relevance can be summarized as follows.

1. *Inflation.* Following an early period of exponentially rapid expansion and particle production, initial quantum fluctuations manifested themselves as perturbations in the densities and bulk velocities of matter fields in the energy momentum tensor. By Einstein's equations these fluctuations give rise to gravitational potentials which perturb the background metric.

2. *Big Bang Nucleosynthesis (BBN).* As the Universe expanded and the temperature dropped, the light elements ^{2}H, ^{3}He, ^{4}He, and ^{7}Li were formed by a series of nuclear reactions, with final abundances relative to hydrogen which are largely determined by the baryon–to–photon ratio, $\eta_{B\gamma}$, but also by the effective number of neutrino species N_ν.

3. *Acoustic oscillations.* Before the time of last scattering and during recombination the Thomson scattering of electrons and CMB photons facilitated the transfer of energy and momentum between these species, and also between CMB photons, protons and other charged light nuclei. The series of peaks and troughs seen in the CMB power spectrum today arise from the acoustic oscillations that propagated through the plasma of electrons, protons and CMB photons in this era. The 13.6 eV binding energy of hydrogen restricts the amplification or diminution of the amplitude of the acoustic waves in the primordial plasma.

4. *Reionization.* After recombination the direct mechanism of photon–electron scattering which alters CMB photon energies stopped until the Universe was once again ionized by the bursts of radiation from the formation of the first stars. The imprint left on the CMB anisotropy spectrum from reionization is comparatively marginal, featuring principally as a reduction in amplitude which does not change other salient features.

5. *Propagation through intervening structures.* Our observations of the CMB temperature anisotropies depend on the propagation of photons over the entire period from last scattering until today. Photon geodesics are affected both by the background cosmology, and the deviations from the background due to the growth of structure. One key effect is the *late time integrated Sachs–Wolfe (ISW) effect*: when CMB photons traverse a region where the gravitational potential changes over time, the boost in energy when CMB photons fall into a potential well is not canceled by the reduction in energy when the photons climb out of the potential well. This has a significant effect for large angles in the anisotropy spectrum.

   The power spectrum is also affected by a number of secondary effects caused by cosmic structures, including the Sunyaev-Zel'dovich effect, weak gravitational lensing and changes to photon polarization. In this paper, however, we are simply concerned with the primary anisotropies.

Within a specific FLRW model the features seen in the CMB power spectrum can be attributed to the relative magnitudes of the various parameters including: the Hubble constant, H_0, and the density parameters of all nonrelativistic matter, Ω_{M0}; baryons, Ω_{B0}; all radiation species, Ω_{R0}; photons, $\Omega_{\gamma 0}$; scalar curvature, Ω_{k0}; and dark energy, $\Omega_{\Lambda 0}$.

A physical understanding of the features of the CMB anisotropies was made possible by the semi–analytic methods first developed by Hu and Sugiyama [32], and later on replicated and refined by numerous other authors [33–35]. A concise exposition can be found in [36], the key point relevant to our discussion of CMB anisotropies in the timescape cosmology being the following.

(i) The location of the first peak of the CMB temperature power spectrum in multipole space depends on the angle $\theta = d_s(t_{\rm dec})/d_A(t_{\rm dec})$ at which the sound horizon is seen today. The angular diameter distance to the last scattering surface[1]

$$d_A(t_{\rm dec}) = \frac{a(t_{\rm dec})\,c}{a_0 H_0 |\Omega_{\rm k0}|^{1/2}}\,{\rm sinn}\left[|\Omega_{\rm k0}|^{1/2}\int_0^{z_{\rm dec}}\frac{H_0\,{\rm d}z}{H}\right]$$

depends on the expansion rate and can change substantially with changes in $\Omega_{\Lambda 0}$, $\Omega_{\rm k0}$, and H_0. The proper scale of the sound horizon $d_s(t) = a(t)\int_0^t c_s {\rm d}t/a$ is changed when $\Omega_{\rm B0}$, $\Omega_{\rm M0}$ and $\Omega_{\rm R0}$ are changed.

(ii) The peaks and troughs in the power spectrum arise from constructive and destructive interference of the sound waves in the baryon–photon fluid. This interference is not exactly in phase or out of phase and the resulting ratios of odd to even peaks depend on $\Omega_{\rm B0}/\Omega_{\gamma 0}$ (or equivalently on $\eta_{B\gamma}$ the baryon-to-photon ratio) that determine the relative phase of the oscillating waves.

(iii) On small angular scales, or equivalently for large multipoles, $\ell \sim (k/a)d_A$, the CMB photons can diffuse and wash away anisotropies. This is apparent as a decaying of the CMB power spectrum amplitude as the multipole moments increase. In the hydrodynamic limit, with the energy momentum tensor taken to be that of an imperfect fluid, this damping of sound waves for wavelengths smaller than the diffusion length

$$\lambda_d^2 = a_L^2\int_0^{t_L}\frac{1}{6a^2(1+R)\sigma_{\rm T}n_e}\left\{\frac{16}{15}+\frac{R^2}{(1+R)}\right\}c\,{\rm d}t$$

is due to viscosity and heat conduction in the baryon–photon plasma. Here $R = (3/4)\rho_B/\rho_\gamma$, $\sigma_{\rm T}$ is the Thomson cross section and n_e is the number density of free electrons. The power spectrum at a given multipole is damped by a factor

$$\exp\left(-\frac{k^2}{a^2}\lambda_d^2\right) \approx \exp\left(-\frac{\ell^2}{d_A^2}\lambda_d^2\right)\,.$$

The parameters $\Omega_{\rm B0}$, $\Omega_{\rm M0}$, $\eta_{B\gamma}$ modify the power spectrum by changing d_A and λ_d in the damping factor.

(iv) The influence of reionization is to suppress the power spectrum by a factor $\exp(-\tau_{\rm reion})$, where the optical depth $\tau = \int \sigma_{\rm T} n_e\,{\rm d}t$ is evaluated at the reionization epoch. With the exception of very small multipoles the rescaling is $C_\ell^{\rm obs} \to \exp(-2\tau_{\rm reion})C_\ell^{\rm obs}$.

(v) The overall amplitude of the power spectrum is proportional to the amplitude A_s of the primordial perturbations. In this paper we use the high-ℓ Planck power spectrum data $\ell \geq 50$ and for these multipoles the reionization effect is degenerate with the primordial perturbation amplitude because the product $\exp(-\tau_{\rm reion})A_s$ multiplies the power spectrum.

(vi) The power spectrum is calculated by convolving the temperature multipoles Θ_ℓ with the primordial spectrum and integrating over all Fourier modes

$$C_\ell = \frac{1}{2\pi}A_s\int\frac{dk}{k}\left[\Theta_\ell(t_0,k)\right]^2\left(\frac{k}{k_0}\right)^{n_s-1}\,.$$

For small values of ℓ (large angles) the temperature multipoles are only related to the monopole at recombination and the integral can be performed analytically. For spectral index $n_s = 1$, $C_\ell \sim 1/[\ell(\ell+1)]$. This scaling is visible as the Sachs-Wolfe plateau. For $n_s < 1$, $C_\ell \sim 1/[\ell^{n_s}(\ell+1)]$ and there is more power at these multipoles compared to the case of $n_s = 1$. In general the effect of n_s on the CMB power spectrum is neither a simple shifting of the peaks nor a simple change in amplitude.

B. Exact inhomogeneous models

In a step up in complexity from the homogeneous isotropic FLRW solutions the CMB has been also been studied in the spherically symmetric but inhomogeneous LTB model [22–24]. On small scales this solution is an excellent approximation for the voids [13–15, 18] that dominate the Universe at the present epoch. Applied to gigaparsec scales the solution becomes a toy model that is physically unlikely, and which violates the Copernican principle. Nonetheless, being an exact solution of the Einstein field equations, it is amenable to direct analytic study, and such studies have included the investigation of the CMB for gigaparsec voids [37–41].

The LTB solutions have a dust energy–momentum tensor, and can only apply at epochs in the matter–dominated era. An early time spherically symmetric radiation plus matter background which evolves to an LTB solution is beyond the realm of current investigations. Consequently, the study of CMB anisotropies in LTB cosmologies has to date used models which initially coincide with a FLRW model. The primary temperature anisotropies are evolved using the Boltzmann hierarchy

[1] Here ${\rm sinn}(x) \equiv \{\sin(x),\ \Omega_{\rm k0} < 0;\ x,\ \Omega_{\rm k0} = 0;\ \sinh(x),\ \Omega_{\rm k0} > 0\}$.

with a FLRW background at early times and the resulting CMB power spectrum is then modified to account for differences in expansion rate, matter densities and angular diameter distances between the FLRW and LTB background solutions [37–41].

Since the timescape model is close to a FLRW model at early times, we will adopt a similar approach in this paper. Specifically we will adapt the method outlined in [42], in which it is shown that the CMB power spectra in two different models can be mapped onto each other as follows.

Consider two cosmological models with angular diameter distances d'_A and d_A and a common proper length scale L at the surface of last scattering. This is viewed at an angle $\theta' = L/d'_A$ and $\theta = L/d_A$ respectively in the two models. Vonlanthen, Räsänen and Durrer [42] show that the CMB angular power spectra in these models are related via the integral

$$C_\ell = \sum_{\tilde\ell} \frac{2\tilde\ell+1}{2} C'_{\tilde\ell} \int_0^\pi \sin\theta \, \mathrm{d}\theta \, P_{\tilde\ell} \left[\cos(\theta \, d_A/d'_A)\right] P_\ell(\cos\theta). \tag{3}$$

Eq. (3) is derived using the assumption that apart from the overall amplitude of the two CMB power spectra, the only differences between the two spectra are due to the differences in the distance to the surface of last scattering characterized by d'_A and d_A. Furthermore, for high multipoles ($\ell \geq 50$) Vonlanthen, Räsänen and Durrer [42] show that (3) can be approximated as

$$C_\ell \approx \left(\frac{d'_A}{d_A}\right)^2 C'_{\frac{d'_A}{d_A}\ell} \, . \tag{4}$$

Let us refer to the cosmology with d'_A as a *reference model*. Then the C_ℓ in the second model at any multipole ℓ is found from the scaled $\tilde\ell = \ell \, d'_A/d_A$ of the reference model. Zibin, Moss and Scott [43] first derived (4) using a different method and the revised results in [44] also agree with (4).

III. CMB ANISOTROPY OVERVIEW FOR THE TIMESCAPE MODEL

We will use (4) to calculate the CMB power spectrum in the timescape model from a reference FLRW power spectrum. In doing so, we must implicitly assume that the key features of the CMB anisotropy spectrum are close to those of a FLRW model apart from the shift factor. In particular, we neglect:

(i) the effects of backreaction on average cosmic evolution in the radiation–dominated epoch [31];

(ii) differences in the late time ISW effect between the timescape and FLRW models.

Even if the timescape model is close to a FLRW model in the radiation dominated epoch, the detailed treatment of the late time ISW effect may differ. However, this might be expected to only affect large angle multipoles ($\ell \lesssim 50$), and we will not include these multipoles in fitting the Planck data.

Our method of determining an appropriate FLRW reference model is complicated by the fact that in the timescape scenario one is not dealing with a single set of cosmological parameters common to all observers. In the presence of inhomogeneity there is more than one single class of average observers, and in general there are both bare and dressed cosmological parameters [45, 46]. We will first briefly review the details of the relationship between bare and dressed parameters in the timescape model, and then describe how the methodology of Sec. II is modified to find reference FLRW models, whose expansion history from last scattering until the present is closest to that of the timescape scenario.

A. Cosmological parameters in the timescape scenario

We follow Ref. [8] in considering a universe containing nonrelativistic matter plus radiation (photons and neutrinos), of respective densities $\rho_{\rm M}$ and $\rho_{\rm R}$, whose evolution is governed by the Buchert equations [30, 31]. The radiation pressure $P_{\rm R} = \frac{1}{3}\rho_{\rm R}c^2$ is assumed to commute under the Buchert average[2] [30],

$$\partial_t \langle P_{\rm R}\rangle - \langle \partial_t P_{\rm R}\rangle = \langle P_{\rm R}\vartheta\rangle - \langle P_{\rm R}\rangle\langle\vartheta\rangle = 0, \tag{5}$$

throughout the evolution of the Universe, so that it is solely the growth of gradients in the nonrelativistic matter density which drives the growth of inhomogeneity in the Universe and backreaction on average cosmic evolution as compared to a FLRW model. The present epoch horizon volume, $\mathcal{V} = \mathcal{V}_{\rm i}\bar{a}^3$, is assumed to be a statistical ensemble of disjoint void and wall regions characterized by respective scale factors $a_{\rm v}$ and $a_{\rm w}$, which are related to the volume–average scale factor by

$$\bar{a}^3 = f_{\rm vi}{a_{\rm v}}^3 + f_{\rm wi}{a_{\rm w}}^3. \tag{6}$$

Here $f_{\rm vi}$ and $f_{\rm wi} = 1 - f_{\rm vi}$ represent the fraction of the initial volume, $\mathcal{V}_{\rm i}$, in void and wall regions respectively at an early unspecified epoch. If one defines $f_{\rm w}(t) = f_{\rm wi}{a_{\rm w}}^3/\bar{a}^3$ to be the *wall volume fraction*, and $f_{\rm v}(t) = f_{\rm vi}{a_{\rm v}}^3/\bar{a}^3$ the *void volume fraction*, then (6) may be rewritten as

$$f_{\rm v}(t) + f_{\rm w}(t) = 1. \tag{7}$$

[2] Here ϑ is the expansion scalar and angled brackets denote the spatial volume average of a scalar quantity on the surface of average homogeneity, so that $\langle P_{\rm R}\rangle \equiv \left(\int_{\mathcal{D}} \mathrm{d}^3x\sqrt{\det {}^3g}\, P_{\rm R}(t,\mathbf{x})\right)/\mathcal{V}(t)$, where $\mathcal{V}(t) \equiv \int_{\mathcal{D}} \mathrm{d}^3x\sqrt{\det {}^3g}$ is the average spatial volume, ${}^3g_{ij}$ being the 3-metric. The domain $\mathcal{D}$ is taken to be the particle horizon volume in our case.

The voids are assumed to have negative spatial curvature characterized by $\langle\mathcal{R}\rangle_{\rm v} \equiv 6k_{\rm v}c^2/{a_{\rm v}}^2$ with $k_{\rm v} < 0$, while wall regions [1] are on average spatially flat, $\langle\mathcal{R}\rangle_{\rm w} = 0$.

With these assumptions the independent Buchert equations may be written as [8]

$$\bar{\Omega}_M + \bar{\Omega}_R + \bar{\Omega}_k + \bar{\Omega}_{\mathcal{Q}} = 1, \tag{8}$$

$$\ddot{f}_{\rm v} + \frac{{\dot{f}_{\rm v}}^2(2f_{\rm v}-1)}{2f_{\rm v}(1-f_{\rm v})} + 3\dot{f}_{\rm v}\bar{H} - \frac{3}{2}(1-f_{\rm v})\bar{\Omega}_k\bar{H}^2 = 0, \tag{9}$$

where

$$\bar{H} \equiv \frac{\dot{\bar{a}}}{\bar{a}} = f_{\rm w}H_{\rm w} + f_{\rm v}H_{\rm v}\,, \tag{10}$$

with $H_{\rm w} \equiv \dot{a}_{\rm w}/a_{\rm w}$ and $H_{\rm v} \equiv \dot{a}_{\rm v}/a_{\rm v}$. We describe $\bar{H}$ as the *bare* or *volume–average* Hubble parameter and

$$\bar{\Omega}_M = \frac{8\pi G\bar{\rho}_{M0}\bar{a}_0^3}{3\bar{H}^2\bar{a}^3}\,, \tag{11}$$

$$\bar{\Omega}_R = \frac{8\pi G\bar{\rho}_{R0}\bar{a}_0^4}{3\bar{H}^2\bar{a}^4}\,, \tag{12}$$

$$\bar{\Omega}_k = \frac{\alpha^2{f_{\rm v}}^{1/3}}{\bar{a}^2\bar{H}^2}\,, \tag{13}$$

$$\bar{\Omega}_{\mathcal{Q}} = \frac{-{\dot{f}_{\rm v}}^2}{9f_{\rm v}(1-f_{\rm v})\bar{H}^2}\,, \tag{14}$$

are the *bare* or *volume–average* density parameters of nonrelativistic matter, radiation, average spatial curvature and kinematic backreaction[3] respectively. Here $\alpha^2 \equiv -k_{\rm v}c^2{f_{\rm vi}}^{2/3} > 0$.

Apart from the presence of the backreaction term, $\bar{\Omega}_{\mathcal{Q}}$, one key difference from the FLRW model is that the curvature parameter $\bar{\Omega}_k$ does not scale simply in proportion to $(\bar{a}\bar{H})^{-2}$; i.e., cosmic expansion does not preserve average spatial curvature. This leads to important phenomenological differences from the FLRW models, both in the timescape scenario [1]–[8] and in other approaches [47]–[49] to backreaction. The nonrigid evolution of the average spatial curvature is subject to a cosmological test [50], for which current observational bounds [51] are consistent with the timescape scenario.

The bare density parameters (11)–(14) are fractions of the critical density, $\bar{\rho}_{\rm cr} = 3\bar{H}^2/(8\pi G)$, in terms of the volume–average Hubble parameter, and the time derivative in (8)–(14) is the volume–average, or bare, Buchert time parameter which best describes average cosmic evolution. In the timescape scenario this time parameter is operationally understood to only coincide with the clock of an isotropic observer[4] whose local regional density coincides with the particle horizon volume average density $\langle\rho\rangle$. On account of a relative volume deceleration, this time parameter is not generally synchronous with the clocks of other isotropic observers for whom the locally isotropic regional density is different.

Observers in bound systems are necessarily in regions which are locally greater than critical density, and can be always be enclosed in compact *finite infinity* surfaces which are marginally expanding at the boundary but within which the average expansion is zero, and average spatial curvature is zero [1]. The volume bounded by the union of these surfaces defines the wall regions discussed above. While the wall regions are always expanding less quickly than the voids, as measured by any one set of clocks, so that

$$h_r \equiv H_{\rm w}/H_{\rm v} < 1\,, \tag{15}$$

the timescape model embodies the physical principle that in the statistical geometry one can always make a choice of rulers and clocks to make the expansion uniform [4].

Clocks of isotropic observers in the denser wall regions, which experience greater regional volume deceleration, run slower relative to those in less dense void regions. With this condition the clocks of wall observers are found to keep *wall time*, $\mathrm{d}\tau_{\rm w} = \mathrm{d}t/\bar{\gamma}$, where

$$\bar{\gamma} = 1 + \left(\frac{1-h_r}{h_r}\right)f_{\rm v} \tag{16}$$

is the *phenomenological lapse function*. Since $\bar{\Omega}_{\mathcal{Q}} = -(1-f_{\rm v})(1-\bar{\gamma})^2/[f_{\rm v}\bar{\gamma}^2]$, from (8) it follows that the phenomenological lapse function is related to the bare density parameters at any epoch by[5]

$$\bar{\gamma} = \frac{\sqrt{1-f_{\rm v}}\left[\sqrt{1-f_{\rm v}} + \sqrt{f_{\rm v}(\bar{\Omega}-1)}\,\right]}{1-f_{\rm v}\bar{\Omega}}\,, \tag{17}$$

where

$$\bar{\Omega} \equiv 1 - \bar{\Omega}_{\mathcal{Q}} = \bar{\Omega}_M + \bar{\Omega}_R + \bar{\Omega}_k\,. \tag{18}$$

In [1] a radial null geodesic matching procedure is implemented to determine effective dressed cosmological parameters inferred by wall observers, such as ourselves, who mistakenly assume that our regional spatially flat geometry extends to the entire Universe. The dressed Hubble parameter is found to be

$$H = \bar{\gamma}\bar{H} - \bar{\gamma}^{-1}\dot{\bar{\gamma}}\,, \tag{19}$$

[3] The kinematic backreaction $\mathcal{Q} \equiv \frac{2}{3}\left(\langle\vartheta^2\rangle - \langle\vartheta\rangle^2\right) - 2\langle\sigma^2\rangle$ includes a contribution from the shear scalar, $\sigma^2 = \frac{1}{2}\sigma_{\alpha\beta}\sigma^{\alpha\beta}$, in general. We assume this to be negligible in cosmic averages, so that the backreaction is determined solely by the variance in volume expansion between walls and voids. One then finds $\mathcal{Q} = 2{\dot{f}_{\rm v}}^2/[3f_{\rm v}(1-f_{\rm v})]$.

[4] An isotropic observer is one who is understood to see a CMB sky which is as close to isotropic as possible.

[5] This corrects a typographical error in Eq. (22) of [8].

with a present epoch value that corresponds to the Hubble constant determined on scales larger than the statistical homogeneity scale ($\gtrsim 100\,h^{-1}$Mpc).

One can similarly define a dressed matter density parameter $\Omega_{\rm M} \equiv \bar{\gamma}^3\bar{\Omega}_M$ which takes a numerical value closer to the corresponding parameter for the concordance ΛCDM model when evaluated at the present epoch. However, it is just a convenient parametrization and cannot be exactly identified with the FLRW parameter – in particular, dressed density parameters do not constitute a set with values that add up to one as in the case of the bare parameters.

Many details of further cosmological tests and parameter estimates are given in [3].

B. Calibrating CMB anisotropies

With our ansatz for the statistical ensemble of walls and voids, and initial conditions consistent with the amplitude of density perturbations inferred from the CMB, it turns out that at any instant the magnitudes of the bare density parameters in (8) do not differ vastly from those of *some* Friedmann model. For example, for typical solutions [8] at last scattering the void fraction is tiny, $f_{\rm v} \sim 2\times 10^{-5}$ and $\bar{\Omega}_{\mathcal{Q}} \sim -1\times 10^{-5}$.

The void fraction grows considerably over time, and backreaction grows in amplitude as the voids overtake the walls by volume, but it then subsequently decreases and its amplitude is bounded by $|\bar{\Omega}_{\mathcal{Q}}| < 0.043$. Over very small time periods there is a "closest Friedmann model" in volume–average time. However, given a backreaction term with a magnitude at the few percent level, and a nonrigidly scaling curvature parameter, the overall time evolution does differ very significantly from any single FLRW model without dark energy over long time scales.

Since $|\bar{\Omega}_{\mathcal{Q}}| \lesssim 10^{-5}$ up to last scattering, it seems reasonable to expect that the physics of the early Universe is little changed in determining the acoustic oscillations in the plasma, or any earlier processes. In determining a reference FLRW model for applying (4) there are two important considerations:

- Since the equations (8), (9) which are closest to the Friedmann equations are statistical equations in volume–average time, the calibration of the relevant parameters in the early Universe in relation the observations of observers who measure wall time (such as ourselves) has to be carefully considered.

- To apply any existing CMB anisotropy code a reference FLRW model has to be found, whose expansion history evaluated at the present day relative to last scattering is the closest to the expansion history of a solution to (8), (9) as determined by a volume–average observer.

Let us first consider each of the epochs listed in Sec. II A in relation to the question of calibration of parameters.

1. *Inflation.* The timescape model assumes the phenomenology of inflationary models and their predictions for the spectrum of density perturbations up to last scattering. The fact that the Universe does not evolve by the Friedmann equation after last scattering means that the usual tight bounds which are often assumed to apply to the root mean square density contrast $\delta\rho/\rho(t)$ on scales at late epochs no longer apply, and this quantity can reach values of 6–8% on arbitrarily large scales by the present epoch [4, 12, 21]. However, this does not directly affect measurements of the CMB anisotropy spectrum.

2. *Big bang nucleosynthesis.* There are no changes to BBN physics. However, a key parameter in determining BBN rates and subsequent light element abundances is the baryon–to–photon ratio, $\eta_{B\gamma}$. In the timescape scenario, on account of the large gradients in spatial curvature between voids and walls and the different relative clocks to which the frequency of a photon is compared, a volume–average isotropic observer will infer mean CMB temperature, $\bar{T}$, which differs from that of a wall observer according to
$$\bar{T} = \bar{\gamma}^{-1}T\,, \qquad (20)$$
at any epoch. In particular, at the present epoch volume–average temperature $\bar{T}_0 = \bar{\gamma}_0^{-1}2.7255\,{\rm K}$ will be up to about 35% cooler. This recalibration of volume–average parameters changes the constraints resulting from light element abundances. In particular, for observational tests performed to date [5, 8] it was possible to find a best fit with a volume–average baryon–to–photon ratio, $\eta_{B\gamma}$, which avoids a primordial lithium abundance anomaly [52, 53].

3. *Acoustic oscillations.* There are no changes to the physics governing the acoustic oscillations since the effects of backreaction are neglected in the early Universe. However, since $\eta_{B\gamma}$ may be recalibrated cosmological parameters relevant to the determination of spectral features – in particular, the ratio of nonbaryonic CDM to baryonic matter, $\Omega_{\rm C0} = (\Omega_{\rm M0} - \Omega_{\rm B0})/\Omega_{\rm B0}$ – may differ from FLRW–model values. As the ^{4}He abundance is potentially changed, this must also be accounted for in the recombination code.

4. *Reionization.* In this paper we do not assume any differences relative to a perturbative FLRW model calibrated by the timescape parameters.

5. *Propagation through intervening structures.* The dressed timescape geometry [1, 3, 8] is used to determine the angular diameter distance of the sound

horizon, and any other average observational quantities. In addition to changing the average expansion history, it is very possible that quantities such as the amplitude of the late time ISW effect may also differ between the timescape cosmology and the standard ΛCDM cosmology. However, this will be neglected here; only small angle multipoles $\ell > 50$ will be used in fitting the Planck data.

C. Matching volume–average expansion history to a FLRW model

Since the expansion history in volume–average time is assumed to be close to that of a FLRW cosmology in the early Universe, and since it is physical processes up to the decoupling and baryon drag epochs which are principally responsible for the observed acoustic peaks, we will aim to adapt standard numerical codes as far as is possible. However, even though the relevant physical processes occur in the early Universe, standard codes for determining the acoustic peaks are calibrated to cosmological parameters, such as H_0, $\Omega_{\rm M0}$, $\Omega_{\Lambda 0}$ etc which are evaluated at the present epoch. These are related to the physical parameters in the early Universe assuming the expansion history of a FLRW model. Most significantly, the perturbation equations used as the basis of the Boltzmann hierarchy use a single global background FLRW geometry, which is written in terms of present epoch cosmological parameters.

Replacing the expansion history of the FLRW model by that of the timescape model would require rewriting almost all codes from scratch, a mammoth task which is not easily realizable considering the decades of effort that have resulted in codes such as CAMB [54] and CLASS [55, 56]. We therefore adopt the approach of determining the acoustic peaks from a FLRW model with scale factor $\hat{a}$, whose expansion history most closely matches that of the volume–average statistical geometry. This approach is justified since it is the volume–average geometry whose expansion history describes average cosmic evolution in the sense closest to the FLRW models. Using the exact timescape solution [8] we can estimate the difference in cosmological parameters at the epoch of decoupling.

In all cases we will match solutions by determining a FLRW solution for which

$$\frac{\hat{a}_0}{\hat{a}} = \frac{\bar{a}_0}{\bar{a}} = 1 + \bar{z} \qquad (21)$$

at all epochs, but with a Hubble parameter which differs in general, $\hat{H} \neq \bar{H}$, meaning that the timescape matter and radiation density parameters (11) and (12) will in general differ from those of the matched FLRW model. However, we will always arrange the matching so that $\hat{H} \simeq \bar{H}$ at early times. At late times we have the freedom to choose some parameters of the matched FLRW model to be equal to those of the timescape model at *one* epoch. Our choice will be to make the present epoch Hubble constant, matter and radiation parameters of the matched model (hatted variables) all equal to the corresponding bare parameters in the timescape model:

$$\hat{H}_0 = \bar{H}_0 \qquad (22)$$

$$\hat{\Omega}_{\rm M0} = \bar{\Omega}_{\rm M0} \qquad (23)$$

$$\hat{\Omega}_{\rm R0} = \bar{\Omega}_{R0}. \qquad (24)$$

This ensures that matter–radiation equality occurs at the same (bare) redshift, $\bar{z}$, in the timescape model as in the FLRW counterpart. Since the baryonic matter density parameter scales in proportion to the matter density parameter, it also follows that

$$\hat{\Omega}_{\rm B0} = \bar{\Omega}_{\rm B0}. \qquad (25)$$

Furthermore, since the Hubble constants are matched at the present epoch, we have $\hat{\Omega}_{\rm M0}\hat{h}^2 = \bar{\Omega}_{\rm M0}\bar{h}^2$, $\hat{\Omega}_{\rm B0}\hat{h}^2 = \bar{\Omega}_{\rm B0}\bar{h}^2$ and $\hat{\Omega}_{\rm R0}\hat{h}^2 = \bar{\Omega}_{R0}\bar{h}^2$, which are parameter combinations typical in the standard FLRW model. With these choices the present epoch CMB temperature of the FLRW model also matches the volume–average value $\hat{T}_0 = \bar{T}_0 = \bar{\gamma}_0^{-1} T_0$, which is related to $\hat{\Omega}_{\rm R0}$ in the standard fashion,

$$\hat{\Omega}_{\rm R0} = \frac{32\sigma_{\rm B}\pi G}{3c^3\hat{H}_0^2}\left[1 + \frac{7}{8}\left(\frac{4}{11}\right)^{4/3} N_{\rm eff}\right]\hat{T}_0^4, \qquad (26)$$

where $\sigma_{\rm B}$ is the Stefan–Boltzmann constant and $N_{\rm eff}$ is the effective number of neutrino species.

If we assume that the matching FLRW model is the most general model possible with both curvature and cosmological constant parameters satisfying

$$\hat{\Omega}_{\rm M} + \hat{\Omega}_{\rm R} + \hat{\Omega}_{\rm k} + \hat{\Omega}_{\Lambda} = 1, \qquad (27)$$

then combining (27) with (22) and (23) at the present epoch we find

$$\hat{\Omega}_{\Lambda 0} = 1 - \hat{\Omega}_{\rm k0} - \bar{\Omega}_{\rm M0} - \bar{\Omega}_{R0}. \qquad (28)$$

This places one constraint on $\hat{\Omega}_{\rm k0}$ and $\hat{\Omega}_{\Lambda 0}$, leaving one further constraint to be found to completely fix the matched FLRW model.

In general, once matter–radiation equality is fixed to be the same in the two models then $\hat{H} \simeq \bar{H}$ at all early times when the matched FLRW equation (27) and the first Buchert equation (8) are both dominated by the matter and radiation densities, with $\hat{\Omega}_{\rm M} \simeq \bar{\Omega}_M$ and $\hat{\Omega}_{\rm R} \simeq \bar{\Omega}_R$. However, there are necessarily small differences in these parameters given the differences of the other density parameters appearing in (8) and (27). Different choices of the final matching constraint are found to give differences of magnitude $\delta\hat{\Omega} < 10^{-4}$ in the matched density parameters at decoupling. We have investigated the following choices (labeled "A" for *average* expansion history matching):

1. Model A($\bar{H}_{\rm dec}$): Hubble parameter matched exactly at decoupling

We can choose the Hubble parameters of the two models to be *exactly* equal at any one particular early time redshift. Let us match the Hubble parameters at decoupling. Since we already have the condition (22) this further constraint ensures that the Universe has decelerated by the precisely the same amount from decoupling until the present epoch in the matched FLRW model as in the volume–average geometry of the timescape model.

Equating $\hat{H}_{\rm dec} = \bar{H}_{\rm dec}$ and evaluating (27) at decoupling we have

$$\bar{h}_{\rm dec}^{-2} \left(\hat{\Omega}_{\Lambda 0} + \hat{\Omega}_{\rm k0} \bar{x}_{\rm dec}^2 + \bar{\Omega}_{\rm M0} \bar{x}_{\rm dec}^3 + \bar{\Omega}_{R0} \bar{x}_{\rm dec}^4 \right) = 1 \,, \quad (29)$$

where $\bar{h}_{\rm dec} \equiv \bar{H}_{\rm dec}/\bar{H}_0$, and $\bar{x}_{\rm dec} = \bar{a}_0/\bar{a}_{\rm dec} = 1 + \bar{z}_{\rm dec} = \bar{\gamma}_0(1+z_{\rm dec})/\bar{\gamma}_{\rm dec}$, and $\hat{\Omega}_{\Lambda 0}$ is given by (28). We necessarily have $\hat{\Omega}_{\rm k\,dec} < \bar{\Omega}_{\rm k\,dec}$ since $\bar{\Omega}_M + \bar{\Omega}_R + \bar{\Omega}_k = 1 - \bar{\Omega}_{\mathcal{Q}} > 1$ in the timescape case, whereas the FLRW parameters satisfy (27). For a typical example, such as the best fit parameters of Ref. [8], $\bar{\Omega}_{\rm k\,dec} - \hat{\Omega}_{\rm k\,dec} \simeq 1.2 \times 10^{-5}$, about 16% of the (small) value of $\bar{\Omega}_{\rm k\,dec}$.

By (29) the present curvature parameter of the matched model is fixed to be

$$\hat{\Omega}_{\rm k0} = \frac{\bar{h}_{\rm dec}^2 + \bar{\Omega}_{\rm M0}(1 - \bar{x}_{\rm dec}^3) + \bar{\Omega}_{R0}(1 - \bar{x}_{\rm dec}^4) - 1}{\bar{x}_{\rm dec}^2 - 1} \,. \quad (30)$$

2. Model A($\bar{r}_{\mathcal{H}}$): Match of effective bare comoving distance of particle horizon

As discussed in Sec. 6.4 of Ref. [1] the solution, $\bar{r}$, of the averaged Sachs optical equation

$$\ddot{\bar{r}} + \frac{\dot{\bar{a}}}{\bar{a}} \dot{\bar{r}} + \Big(\frac{\dot{f_{\rm v}}^2}{3 f_{\rm v}(1 - f_{\rm v})} - \frac{\alpha^2 {f_{\rm v}}^{1/3}}{\bar{a}^2} \Big) \bar{r} = 0 \quad (31)$$

provides an estimate of the effective comoving scale as would be measured by a volume average observer, and consequently of an effective volume–average angular diameter scale $\langle d_A \rangle = \bar{a}(t)\, \bar{r}(t)\, \delta$ for a fiducial source which subtends an angle δ in its rest frame. In work to date, we have not used this quantity since it is not directly measured at late times. Since it averages over both void and wall regions, as a function of volume–average conformal time, $\bar{\eta}$, it lies in the range $\bar{\eta} \leq \bar{r}(\bar{\eta}) \leq \sinh(\bar{\eta})$, where the bounds correspond to the FLRW limits: (i) $\bar{r}(\bar{\eta}) = \bar{\eta}$ when $f_{\rm v} \equiv 0$, $\dot{f}_{\rm v} \equiv 0$; (ii) $\bar{r}(\bar{\eta}) = \sinh(\bar{\eta})$, when $f_{\rm v} = {\rm const}$, $\dot{f}_{\rm v} \equiv 0$.

For any given timescape parameters, we integrate (31) from $t = 0$ until the present $t = t_0$ to obtain the effective bare comoving distance of the particle horizon, $\bar{r}_{\mathcal{H}}$. FLRW parameter values values $\hat{\Omega}_{\rm k0}$, $\hat{\Omega}_{\Lambda 0}$, are then chosen to simultaneously satisfy (28) and the constraint

$$\bar{r}_{\mathcal{H}} = \sinh \left(\int_0^1 \frac{\hat{\Omega}_{\rm k0}^{1/2}\, {\rm d}y}{\sqrt{\hat{\Omega}_{\Lambda 0} y^4 + \hat{\Omega}_{\rm k0} y^2 + \bar{\Omega}_{\rm M0} y + \bar{\Omega}_{R0}}} \right) , \quad (32)$$

which is the equivalent solution to (31) in the FLRW limit with $f_{\rm v} \equiv 1$ and $\dot{f}_{\rm v} \equiv 0$.

3. Model A($\bar{\eta}_0$): Match of bare conformal time age of the Universe

For any given timescape parameters, we integrate $\bar{\eta} = \int c\, {\rm d}t/\bar{a}$ from $t = 0$ until the present $t = t_0$, to obtain the bare conformal age of the Universe, $\bar{\eta}_0$. FLRW parameter values values $\hat{\Omega}_{\rm k0}$, $\hat{\Omega}_{\Lambda 0}$, are then chosen to simultaneously satisfy (28) and the constraint

$$\bar{\eta}_0 = \int_0^1 \frac{\hat{\Omega}_{\rm k0}^{1/2}\, {\rm d}y}{\sqrt{\hat{\Omega}_{\Lambda 0} y^4 + \hat{\Omega}_{\rm k0} y^2 + \bar{\Omega}_{\rm M0} y + \bar{\Omega}_{R0}}} \,. \quad (33)$$

4. Model A(t_0): Match of the bare age of the Universe

For any given timescape parameters, we determine the age of the Universe in volume–average time, t_0. FLRW parameter values values $\hat{\Omega}_{\rm k0}$, $\hat{\Omega}_{\Lambda 0}$ are then chosen to simultaneously satisfy (28) and the constraint

$$\bar{H}_0 t_0 = \int_0^1 \frac{y\, {\rm d}y}{\sqrt{\hat{\Omega}_{\Lambda 0} y^4 + \hat{\Omega}_{\rm k0} y^2 + \bar{\Omega}_{\rm M0} y + \bar{\Omega}_{R0}}} . \quad (34)$$

5. Model A($\hat{\Omega}_{\Lambda 0} = 0$): $\hat{\Omega}_{\Lambda 0} = 0$

We set $\hat{\Omega}_{\Lambda 0} = 0$ in the matched FLRW model, so that $\hat{\Omega}_{\rm k0}$ is simply given by (28).

6. Comparison of volume–average expansion history matching methods

In Fig. 1 we show the fractional difference in the matter plus radiation densities of the matched FLRW models which satisfy (22)–(25) relative to those of the timescape model, for the example of the best fit parameters from Ref. [8], viz., $H_0 = 61.7\,{\rm km\ sec^{-1}\,Mpc^{-1}}$, $f_{\rm v0} = 0.695$, $\eta_{B\gamma} = 5.1 \times 10^{-10}$. The ratio of combined matter and radiation densities

$$\frac{\hat{\Omega}_{\rm M} + \hat{\Omega}_{\rm R}}{\bar{\Omega}_M + \bar{\Omega}_R} = \frac{1 - \hat{\Omega}_\Lambda - \hat{\Omega}_{\rm k}}{1 - \bar{\Omega}_{\mathcal{Q}} - \bar{\Omega}_k} \quad (35)$$

is initially very close to unity, and in general its departure from unity is a measure of the extent to which the sum of

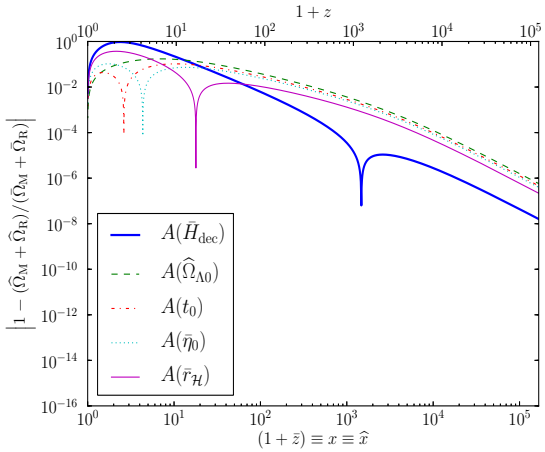

FIG. 1: Fractional difference in the ratio of matter plus radiation densities of the matched FLRW models relative to the volume–average matter plus radiation densities of the timescape model, for the average expansion history matching procedures, using the best fit parameters from Ref. [8].

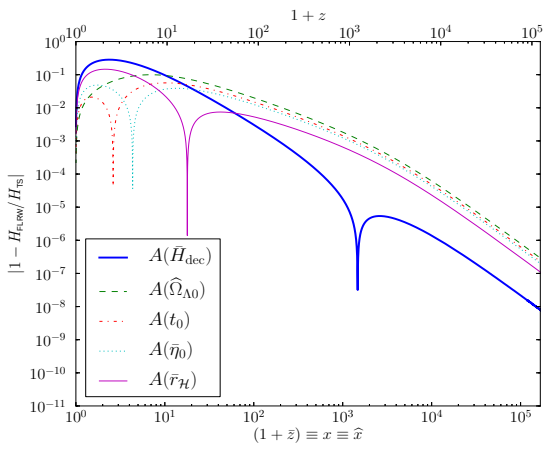

FIG. 2: Fractional difference of the Hubble parameter of the matched FLRW models relative to the volume–average Hubble parameter of the timescape model, for the average expansion history matching procedures, using the best fit parameters from Ref. [8]. For all procedures $\hat{H}_0 = \bar{H}_0$ at the present epoch.

the dark energy and spatial curvature parameters in the matched FLRW model differ from the backreaction and curvature contributions in the timescape model. Model $\mathrm{A}(\bar{H}_{\rm dec})$, which has its final matching condition set at decoupling, has the smallest difference in the early Universe with $\left|1-\left(\hat{\Omega}_{\rm M}+\hat{\Omega}_{\rm R}\right)/\left(\bar{\Omega}_{M}+\bar{\Omega}_{R}\right)\right| \lesssim 10^{-5}$ before decoupling. For the other average expansion history matching methods, which are based on a matching condition set at late epochs, the corresponding difference is typically two orders of magnitude larger before decoupling, which still means a difference of $\lesssim 10^{-3}$.

The $\mathrm{A}(\bar{H}_{\rm dec})$ matching method is also seen to produce a closer match at early times (large redshifts) to quantities such as the volume–average Hubble parameter, expansion age and conformal time as compared to the other matching conditions, as is seen in Figs. 2–4. This is true for redshifts $\bar{z} \gtrsim 70$ (bare) or $z \gtrsim 50$ (dressed). Since the physics of the early Universe is the most crucial for determining the features of the acoustic peaks, we will therefore take model $\mathrm{A}(\bar{H}_{\rm dec})$ as the canonical matching method for determining the fit of the timescape model to the Planck data.

While a general trend of increased departure from FLRW–like behavior can be seen in all matching types, the largest difference in Figs. 1 and 2 for the canonical matched model $\mathrm{A}(\bar{H}_{\rm dec})$ occurs when the backreaction contribution is at its maximum, $|\bar{\Omega}_{\mathcal{Q}}| \simeq 0.043$, in the dressed redshift range $1 \lesssim z \lesssim 5$. (See Fig. 1 in [3] and also Fig. 1 in [8].) Since the impact of an increase in $|\bar{\Omega}_{\mathcal{Q}}|$ on volume–average time and conformal time is not immediate, but rather cumulative, for the $\mathrm{A}(\bar{H}_{\rm dec})$ matched model the fractional difference from unity peaks at a lower redshift, as seen in Figs. 3 and 4, and then drops again once $|\bar{\Omega}_{\mathcal{Q}}|$ decreases.

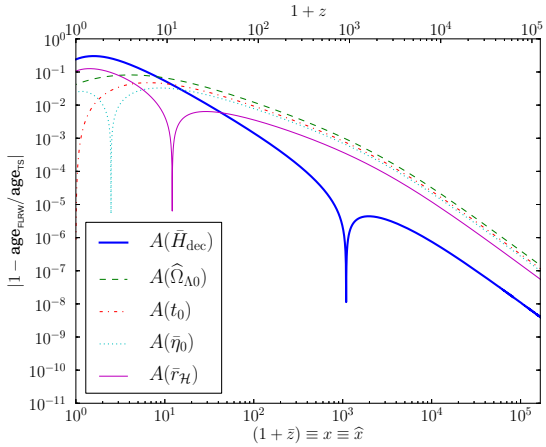

FIG. 3: Fractional difference of the expansion age of the matched FLRW models relative to the volume–average expansion age of the timescape model, for the average expansion history matching procedures, using the best fit parameters from Ref. [8]. The respective present ages, $\hat{t}_0$, of the matched models are: $\mathrm{A}(\bar{H}_{\rm dec})$, 21.7 Gyr; $\mathrm{A}(\bar{r}_{\mathcal{H}})$, 19.2 Gyr; $\mathrm{A}(\bar{\eta}_0)$, 17.9 Gyr; $\mathrm{A}(t_0)$, 17.5 Gyr $(= t_0)$; $\mathrm{A}(\hat{\Omega}_{\Lambda 0} = 0)$, 16.8 Gyr.

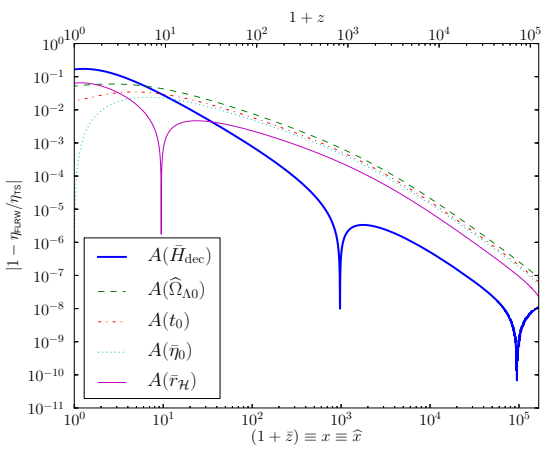

FIG. 4: Fractional difference of the conformal age of the matched FLRW models relative to the volume–average expansion age of the timescape model, for the average expansion history matching procedures, using the best fit parameters from Ref. [8]. The respective present conformal ages, $\hat{\eta}_0$, of the matched models are: A($\bar{H}_{\rm dec}$), 4.06; A($\bar{r}_{\mathcal{H}}$), 3.70; A($\bar{\eta}_0$), 3.48 ($= \bar{\eta}_0$); A(t_0), 3.41; A($\hat{\Omega}_{\Lambda 0} = 0$), 3.30.

D. Matching wall expansion history to a FLRW model

The matching methods of Sec. III C ensure that the expansion history is as close as possible to that of the volume–average expansion history in one sense or another. It is therefore likely to accurately constrain the two free parameters that essentially describe the timescape expansion history, namely the bare Hubble constant, $\bar{H}_0$, and the void fraction, $f_{\rm v0}$, (or equivalently other pairs of independent parameters such as the dressed Hubble constant, H_0, and dressed matter density parameter, $\Omega_{\rm M0}$).

Although the differences in the density parameters of the timescape model are small as compared to the matched FLRW at early epochs, (with $\delta\hat{\Omega} < 10^{-4}$), differences which are small in terms of determining the background may nonetheless be significant in the treatment of the perturbations of the background, which are a significant part of the standard codes which we adopt in the early Universe.

The timescape model incorporates the assumption that the geometry on the finite infinity scale is very close to that of a spatially flat model, becoming close to Einstein–de Sitter at late times. The relevant perturbation theory on finite infinity scales is therefore likely to be closer to that of the spatially flat matter plus radiation solution with no curvature or Λ term.

We will therefore also investigate alternative matching procedures in which the initial conditions at decoupling are as close as possible to those of the timescape model, but the expansion history is constrained to match that of the wall geometry only rather than the volume–average geometry. We will also consider a second model in which we perform a similar matching based on the geometry of void centres only. (These models are labeled "W" for *wall* expansion history matching.)

1. *Model W($k = 0$): Match of wall expansion history*

We construct a spatially flat matter plus radiation model with initial conditions matched as closely as possible to those of the wall geometry by taking density parameters

$$\widetilde{\Omega}_M + \widetilde{\Omega}_R = 1, \tag{36}$$

with respect to a spatially flat FLRW model with scale factor, $\tilde{a}$, and Hubble parameter, $\widetilde{H}$, which are matched so that the physical densities of the matter, $\tilde{\rho}_M = 3\widetilde{H}^2\widetilde{\Omega}_M/(8\pi G)$, and radiation, $\tilde{\rho}_R = 3\widetilde{H}^2\widetilde{\Omega}_R/(8\pi G)$, are equal to those of the timescape model at decoupling. Thus

$$\widetilde{H}_{\rm dec} = \bar{\Omega}_{\rm dec}^{1/2}\, \bar{H}_{\rm dec} \tag{37}$$

$$\widetilde{\Omega}_{M\,\rm dec} = \frac{\bar{\Omega}_{M\,\rm dec}}{\bar{\Omega}_{\rm dec}}, \tag{38}$$

$$\widetilde{\Omega}_{R\,\rm dec} = \frac{\bar{\Omega}_{R\,\rm dec}}{\bar{\Omega}_{\rm dec}}, \tag{39}$$

where

$$\bar{\Omega}_{\rm dec} = \bar{\Omega}_{M\,\rm dec} + \bar{\Omega}_{R\,\rm dec} = 1 - \bar{\Omega}_{\mathcal{Q}\,\rm dec} - \bar{\Omega}_{k\,\rm dec}\,. \tag{40}$$

On account of (37) the expansion of the matched model is very close to the timescape model as decoupling, but slower by an amount $(\bar{H}_{\rm dec} - \widetilde{H}_{\rm dec})/\bar{H}_{\rm dec} < 10^{-4}$.

The expansion of the matched model from matter–radiation equality until decoupling is guaranteed to match that of the timescape model since

$$\frac{\tilde{a}_{\rm eq}}{\tilde{a}_{\rm dec}} = \frac{\widetilde{\Omega}_{R\,\rm dec}}{\widetilde{\Omega}_{M\,\rm dec}} = \frac{\bar{\Omega}_{R\,\rm dec}}{\bar{\Omega}_{M\,\rm dec}}\,. \tag{41}$$

The spatially flat FLRW model with matter and radiation has a Hubble parameter given by

$$\widetilde{H} = \frac{\widetilde{H}_{\rm eq}}{\sqrt{2}} \left(\frac{\tilde{a}_{\rm eq}}{\tilde{a}}\right)^2 \sqrt{1 + \frac{\tilde{a}}{\tilde{a}_{\rm eq}}}\,, \tag{42}$$

while the solution in terms of conformal time $\widetilde{\eta} = c\int \mathrm{d}\tilde{t}/\tilde{a}$ is given by [35]

$$\frac{\tilde{a}}{\tilde{a}_{\rm eq}} = 2\left(\frac{\widetilde{\eta}}{\widetilde{\eta}_*}\right) + \left(\frac{\widetilde{\eta}}{\widetilde{\eta}_*}\right)^2, \tag{43}$$

where $\widetilde{\eta}_*^{-1} = \tilde{a}_{\rm eq}\widetilde{H}_{\rm eq}/(2\sqrt{2}\,c)$. Using (37)–(42) we find that

$$\widetilde{H} = \bar{H}_{\rm dec}\left(\frac{\tilde{a}_{\rm dec}}{\tilde{a}}\right)^{3/2}\sqrt{\bar{\Omega}_{M\,\rm dec} + \bar{\Omega}_{R\,\rm dec}\frac{\tilde{a}_{\rm dec}}{\tilde{a}}}\,. \qquad (44)$$

In a similar fashion to the matching methods of Sec. III C one final condition is required for the model matching. In this case we take the present epoch matched spatially flat FLRW model to match that of the wall geometry in volume average time [1, 2]

$$\widetilde{H}_0 = H_{\rm w0} = \bar{\gamma}_0^{-1}\bar{H}_0, \qquad (45)$$

given that the wall geometry is extremely close to an Einstein–de Sitter geometry in volume–average time at late epochs [2]. As a consistency check, we find numerically that the present epoch expansion age of the matched spatially flat FLRW model matches that of the volume–average age of the Universe in the timescape model.

Combining (44), (45) we find

$$\sqrt{\bar{\Omega}_{M\,\rm dec}\widetilde{x}_{\rm dec} + \bar{\Omega}_{R\,\rm dec}} = \frac{\bar{H}_0\widetilde{x}_{\rm dec}^2}{\bar{\gamma}_0\bar{H}_{\rm dec}}\,, \qquad (46)$$

where $\widetilde{x}_{\rm dec} \equiv \tilde{a}_0/\tilde{a}_{\rm dec}$. The expansion of the matched model until the present epoch is now completely fixed.

The notional present epoch CMB temperature of matched FLRW model is also fixed as $\widetilde{T}_0 = \widetilde{x}_{\rm dec}^{-1}\bar{T}_{\rm dec}$ in terms of the physical temperature $\bar{T}_{\rm dec}$ of the primordial plasma at decoupling. In the actual Universe we see CMB photon geodesics which traverse both wall and void regions. Since the void regions expand faster the expansion from decoupling until today is always larger in the actual Universe than in the matched model here, which only has wall regions. Consequently the observed CMB temperature is always less than the notional $\widetilde{T}_0$.

For computational convenience we note that given a solution $\widetilde{x}_{\rm dec}$ of (46) the present epoch density parameters of the matched model are

$$\widetilde{\Omega}_{M0} = \frac{\bar{\Omega}_{M\,\rm dec}\widetilde{x}_{\rm dec}}{\bar{\Omega}_{M\,\rm dec}\widetilde{x}_{\rm dec} + \bar{\Omega}_{R\,\rm dec}}, \qquad (47)$$

$$\widetilde{\Omega}_{R0} = \frac{\bar{\Omega}_{R\,\rm dec}}{\bar{\Omega}_{M\,\rm dec}\widetilde{x}_{\rm dec} + \bar{\Omega}_{R\,\rm dec}}, \qquad (48)$$

while $\widetilde{\Omega}_{B0}/\widetilde{\Omega}_{M0} = \bar{\Omega}_{\rm B0}/\bar{\Omega}_{\rm M0}$.

2. *Model W($k \neq 0$): Match of wall expansion history with initial curvature*

Finally, another variation of the matching procedure of Sec. III D 1 is to replace (36)–(40) by

$$\widetilde{\Omega}_M + \widetilde{\Omega}_R + \widetilde{\Omega}_k = 0, \qquad (49)$$

where

$$\widetilde{H}_{\rm dec} = \bar{\Omega}_{\rm dec}^{1/2}\,\bar{H}_{\rm dec} \qquad (50)$$

$$\widetilde{\Omega}_{M\,\rm dec} = \frac{\bar{\Omega}_{M\,\rm dec}}{\bar{\Omega}_{\rm dec}}, \qquad (51)$$

$$\widetilde{\Omega}_{R\,\rm dec} = \frac{\bar{\Omega}_{R\,\rm dec}}{\bar{\Omega}_{\rm dec}}, \qquad (52)$$

$$\widetilde{\Omega}_{k\,\rm dec} = \frac{\bar{\Omega}_{k\,\rm dec}}{\bar{\Omega}_{\rm dec}}, \qquad (53)$$

with

$$\bar{\Omega}_{\rm dec} = \bar{\Omega}_{M\,\rm dec} + \bar{\Omega}_{R\,\rm dec} + \bar{\Omega}_{k\,\rm dec} = 1 - \bar{\Omega}_{\mathcal{Q}\,\rm dec}\,. \qquad (54)$$

Once again, the expansion between matter–radiation equality and decoupling, $\tilde{a}_{\rm dec}/\tilde{a}_{\rm eq}$, matches that of the timescape model, but the matched model now has a spatial curvature term.

We are effectively still largely matching the expansion history of the wall geometry, but incorporating an initial negative curvature consistent with the initial conditions, to see whether this leads to any noticeable differences.

One may use the Friedmann equation for the matched FLRW model to determine each of the density parameters $\widetilde{\Omega}_{M0}$, $\widetilde{\Omega}_{R0}$ and $\widetilde{\Omega}_{k0}$ at the present epoch in terms of their values at decoupling, $\widetilde{\Omega}_{M\,\rm dec}$, $\widetilde{\Omega}_{R\,\rm dec}$, $\widetilde{\Omega}_{k\,\rm dec}$, and the redshift factor $\widetilde{x}_{\rm dec} = \tilde{a}_0/\tilde{a}_{\rm dec} \equiv 1 + \tilde{z}$. If one combines the resulting expression with (50)–(54) one finds

$$\widetilde{\Omega}_{M0} = \frac{\bar{\Omega}_{M\,\rm dec}\widetilde{x}_{\rm dec}}{\Delta}, \qquad (55)$$

$$\widetilde{\Omega}_{R0} = \frac{\bar{\Omega}_{R\,\rm dec}}{\Delta}, \qquad (56)$$

$$\widetilde{\Omega}_{k0} = \frac{\bar{\Omega}_{k\,\rm dec}\widetilde{x}_{\rm dec}^2}{\Delta}, \qquad (57)$$

where

$$\Delta \equiv \bar{\Omega}_{k\,\rm dec}\widetilde{x}_{\rm dec}^2 + \bar{\Omega}_{M\,\rm dec}\widetilde{x}_{\rm dec} + \bar{\Omega}_{R\,\rm dec}. \qquad (58)$$

Since there is now a constant negative spatial curvature, which is a feature of neither walls nor voids in the timescape model, there is no appropriate expansion rate to match to at the present epoch. Instead we will take the present epoch expansion age of the matched solution to be the age of the Universe in volume–average time, similarly to the case of Sec. III D 1. This leads to the constraint

$$\bar{H}_{\rm dec}t_0 = \int_0^{\widetilde{x}_{\rm dec}}\frac{u\,{\rm d}u}{\sqrt{\bar{\Omega}_{k\,\rm dec}u^2 + \bar{\Omega}_{M\,\rm dec}u + \bar{\Omega}_{R\,\rm dec}}}\,, \qquad (59)$$

which can be used to solve for $\widetilde{x}_{\rm dec}$ and consequently fully constrain the matched model, with density parameters given by (55)–(58) and present epoch Hubble parameter

$$\widetilde{H}_0 = \bar{H}_{\rm dec}\sqrt{\bar{\Omega}_{k\,\rm dec}\widetilde{x}_{\rm dec}^{-2} + \bar{\Omega}_{M\,\rm dec}\widetilde{x}_{\rm dec}^{-3} + \bar{\Omega}_{R\,\rm dec}\widetilde{x}_{\rm dec}^{-4}}. \qquad (60)$$

This concludes the possible matching procedures we have investigated. There is no equivalent procedure based on the void expansion rate only. The voids initially form a tiny fraction of the volume and are not representative of average conditions. At late epochs the voids dominate by volume, with an expansion law close to that of an empty Milne universe. An empty universe model cannot be used as the basis of perturbation theory, however.

IV. CMB ANALYSIS: COMPUTATIONAL METHODOLOGY

Insofar as the details of the evolution of the primordial plasma in the Universe can be assumed to be given by a standard FLRW model then for multipoles $\ell > 50$ we might expect the matching procedures of Secs. III C, III D to give reasonably accurate quantitative estimates of CMB constraints on timescape model parameters. We therefore use the timescape theoretical CMB temperature power spectrum which we obtain from each matched FLRW model and Eq. (4) with the Planck CMB data [57] to constrain timescape parameters.

To find timescape parameters that fit the Planck CMB temperature power spectrum data [57] we employ Bayesian analysis to obtain parameter constraints with the affine invariant[6] Markov chain Monte Carlo (MCMC) algorithm [61] using its python implementation [62]. We fit the parameters of each matched FLRW universe by computing its CMB power spectrum with the CLASS Boltzmann code [55, 56]. We modified the code to allow for the different parameter ranges with extended bounds, as required by the matched FLRW models.

All FLRW model matching procedures also require that we solve the timescape equations with matter and radiation to find the exact present epoch timescape parameter values, as described in [8]. We must further extend our previous numerical computations [8], as the baryon–to–photon ratio, $\eta_{B\gamma}$, will now also be included as a base parameters for the MCMC analysis. In this section we outline the details of all our numerical computations.

[6] Unlike the traditional Metropolis–Hastings [58] algorithm the affine invariant MCMC algorithm does not require a knowledge of the covariance matrix of the MCMC parameters and has the additional advantage of a high acceptance rate. The algorithm only requires the user to select the initial MCMC values close to the best fit parameters and provide an estimate of the errors in the parameters. The algorithm then explores the full parameter space. In a comparison of the Metropolis–Hastings [59], nested sampling and the affine invariant sampling techniques of Allison and Dunkley [60], the affine invariant algorithm is shown to perform very well.

A. Big bang nucleosynthesis

To date all studies of the timescape model have assumed a range of values for the baryon–to–photon ratio, $\eta_{B\gamma}$, consistent with observed light element abundances that avoid the lithium–7 abundance anomaly [52, 53]. However, $\eta_{B\gamma}$ was not constrained from CMB data. Here we will constrain $\eta_{B\gamma}$ directly from the Planck data. We take $\eta_{B\gamma}$ as an MCMC parameter and treat $h^2\bar{\Omega}_{\rm B0}$ as a derived parameter, in contrast to ΛCDM model studies which commonly use $h^2\Omega_{\rm B0}$ as a base MCMC parameter.

Since FLRW model calibrations are built into the BBN characterization of many standard CMB codes, we perform our own BBN calculations by adapting the *fastbbn* code[63] of Sarkar and co-workers [64, 65]. The code takes $\eta_{B\gamma}$ and $N_{\rm eff}$ as free parameters and determines light element abundances, including the helium fraction, $Y_{\rm p}$ [64, 65]. This value of $Y_{\rm p}$ is then used in the timescape recombination calculation, and is also passed to the Boltzmann code of the matched FLRW model.

Another alternative is to ignore the BBN determination of $Y_{\rm p}$ from $N_{\rm eff}$ and $\eta_{B\gamma}$ altogether and add $Y_{\rm p}$ to the list of MCMC parameters. This way $Y_{\rm p}$ is allowed to vary freely and the Planck CMB data alone set its value. This can be done with $N_{\rm eff}$ fixed or free to vary. We have not investigated this last possibility, which if carried out can be regarded as a consistency check of theoretical BBN predictions.

B. Decoupling and recombination

To determine timescape parameters we numerically integrate the timescape equations with matter and radiation, using methods given in Ref. [8]. We also determine precise values for the redshift of decoupling – both bare $\bar{z}_{\rm dec}$ and dressed $z_{\rm dec}$ – and the dressed angular diameter distance to the last scattering surface at decoupling [1]

$$d_{\rm A\,dec} = \bar{a}_{\rm dec}\bar{\gamma}_{\rm dec}(1-f_{\rm v\,dec})^{1/3}\int_{t_{\rm dec}}^{t_0}\frac{{\rm d}t}{\bar{\gamma}\,(1-f_{\rm v})^{1/3}\,\bar{a}}, \quad (61)$$

which is needed to shift the CMB power spectrum in multipole space and also for matching procedures A($\bar{H}_{\rm dec}$), W($k=0$) and W($k\neq 0$).

In our previous work [8] the effects of helium recombination were not included, and we applied the Saha equation beginning at the end of helium recombination. To produce more accurate results, we wrote a simple recombination code that solves for hydrogen and helium ionization fractions, following methods given in refs. [33, 66, 67], in terms of the volume–average temperature $\bar{T}$ in the timescape model. Our recombination code produces results that are consistent with HyRec [68] and RECFAST [69, 70] when used with a FLRW solution. We code for helium recombination [66, 67] beginning at bare redshift $\bar{z} = 10000$, with the initial helium fraction

determined directly from our own BBN code as the parameters $\eta_{B\gamma}$ and $N_{\rm eff}$ are varied.

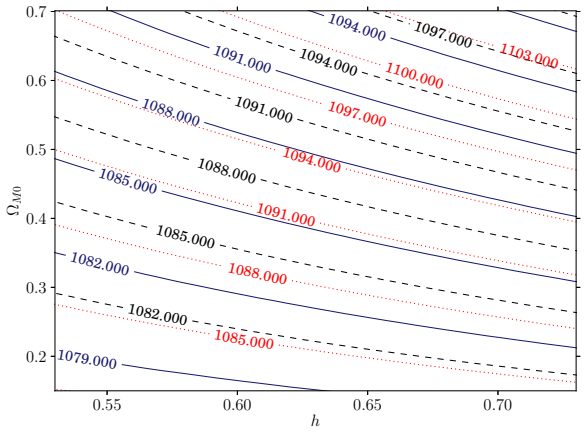

FIG. 5: Contours of dressed redshift of decoupling, $z_{\rm dec}$, in the space of dressed parameters (h, $\Omega_{\rm M0}$), (where $H_0 = 100\,h\,{\rm km\ sec^{-1}\,Mpc^{-1}}$). Contours are shown for the cases $10^{10}\eta_{B\gamma} = 5.1$ (dotted lines), 6.04 (solid lines) and 6.465 (dashed lines).

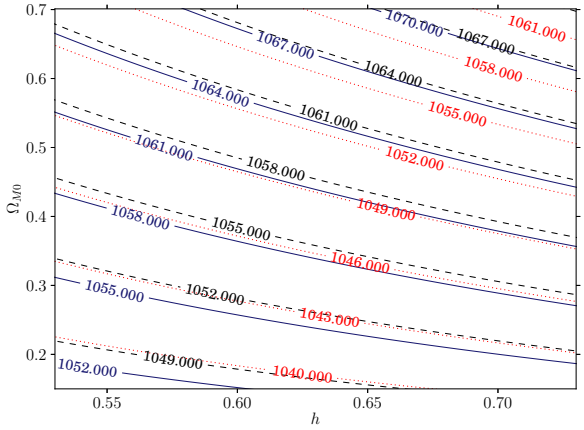

FIG. 6: Contours of the dressed redshift of the baryon drag epoch, $z_{\rm drag}$, in the space of dressed parameters (h, $\Omega_{\rm M0}$), (where $H_0 = 100\,h\,{\rm km\ sec^{-1}\,Mpc^{-1}}$). Contours are shown for the cases $10^{10}\eta_{B\gamma} = 5.1$ (dotted lines), 6.04 (solid lines) and 6.465 (dashed lines).

Including the effects of helium recombination changes the dressed redshift of decoupling slightly as compared to Ref. [8], but has a somewhat more substantial effect on the estimate of the baryon drag epoch. This can be seen in Figs. 5, 6, where we plot contours of $z_{\rm dec}$ and $z_{\rm drag}$ for three values of the baryon–to–photon ratio: $\eta_{B\gamma} = 5.1\times10^{-10}$ as used in Figs. 3 and 4 of Ref. [8], $\eta_{B\gamma} = 6.04\times10^{-10}$ which is a best fit to the ΛCDM model with the Planck data [71], and $\eta_{B\gamma} = 6.465\times10^{-10}$ which is a best fit for fixed $N_{\rm eff} = 3.046$ using the canonical A($\bar{H}_{\rm dec}$) matching method.

C. MCMC parameters and priors

In the top part of Table I we identify the base parameters, i.e., the timescape parameters varied in the MCMC analysis. All other timescape parameters are derived from these. Of the 7 base parameters the 5 parameters $\{f_{\rm v0},\ h,\ T_0 = 2.7255\,{\rm K},\ \eta_{B\gamma},\ N_{\rm eff}\}$ comprise the set that fixes the background timescape model, while the additional two parameters $\{n_{\rm s},\ A_{\rm s}\}$ are needed for the matched perturbed FLRW model. The CMB temperature $T_0 = 2.7255\,{\rm K}$ measured by a wall observer is constrained by observation [72], and is not varied.

We use $N_{\rm eff} = 3.046$ for the base timescape model, as our main aim is to explore the parameter space in the timescape cosmology while remaining consistent with known particle physics[7]. The case in which $N_{\rm eff}$ is left free to vary is discussed in the Appendix.

For other base parameters we choose a wide prior range to explore the full parameter space. Flat priors are chosen, with the exception that the ratio of matter to radiation energy density at decoupling is constrained to be larger than unity, $\bar{\Omega}_{M\,{\rm dec}}/\bar{\Omega}_{R\,{\rm dec}} > 1$, as a strict prior. The range of priors for $f_{\rm v0}$, h are chosen to be larger than their bounds found in previous studies [6, 8].

We assume that the primordial scalar perturbations are adiabatic with a spectrum

$$\mathcal{P}_{\mathcal{R}} = A_{\rm s}\left(\frac{k}{k_0}\right)^{n_{\rm s}-1}, \qquad (62)$$

where we have chosen the pivot scale $k_0 = 0.05\,{\rm Mpc}^{-1}$. We have not investigated alternative initial conditions such as isocurvature scalar perturbations or tensor perturbations, and we set the running of the spectral index ${\rm d}n_{\rm s}/{\rm d}\ln k = 0$.

We treat the amplitude of the power spectrum $A_{\rm s}$ as a nuisance parameter that we cannot constrain. Nevertheless we use a wide prior range for $A_{\rm s}$ to get the normalized power spectrum required by the Planck `CamSpec` likelihood code. We configure the CLASS code to get

[7] Independent of cosmological constraints on $N_{\rm eff}$ a recent compilation [73] of particle physics experiments gives the number of light neutrinos as 2.984 ± 0.008 for experiments that track Z boson production from e^+e^- annihilation, and 2.92 ± 0.05 for experiments that study the $e^+e^- \to \nu\bar{\nu}\gamma$ process. In cosmology, the convention is to parametrize the total radiation energy density parameter by (26). Instead of $N_{\rm eff} = 3$ the value $N_{\rm eff} = 3.046$ is used [74] in (26) to account for noninstantaneous decoupling between electrons/positions and neutrinos, QED corrections to the photon, electron/positron plasma and neutrino flavour oscillations assuming three species of neutrinos.

TABLE I: The timescape parameters varied in MCMC analysis with their assumed priors are shown in the top section. The derived parameters relevant to a volume–average observer are in the middle section and the dressed derived parameters measured by a wall/galaxy observer are shown in the third group. A brief description of the parameters is also given.

Parameter	Prior range	Description
$f_{\rm v0}$	$[0.3, 0.9]$	Fraction of horizon volume in voids today
H_0	$[0.3, 0.9]$	Dressed Hubble parameter
$10^{10}\eta_{B\gamma}$	$[4.0, 7.0]$	$10^{10}\times$ Bare baryon to photon ratio
$N_{\rm eff}$	$[0., 0.6]$	The effective number of neutrino species
$n_{\rm s}$	$[0.9, 1.1]$	Scalar spectrum power-law index, pivot $k_0 = 0.05\,{\rm Mpc}^{-1}$
$10^9 A_{\rm s}$	$[2.0, 20.]$	Amplitude of the primordial curvature perturbations ($k_0 = 0.05$ Mpc^{-1})
T_0		CMB temperature of 2.725K measured by a wall observer
$\left(\bar\Omega_M/\bar\Omega_R\right)_{\rm dec}$	$> 1.$	The ratio of matter to radiation energy density at decoupling
$\bar H_0$		Bare Hubble constant
$\bar T_0$		CMB temperature seen by a volume–average observer
t_0		Age of the Universe (volume–average observer in Gyr)
$\bar\gamma_0$		Present phenomenological lapse function
$Y_{\rm p}$		Helium fraction
$\bar\Omega_{\rm B0}$		Bare baryon density parameter
$\bar\Omega_{\rm C0}$		Bare cold dark matter density parameter
$\bar\Omega_{\rm M0}$		Bare total matter density
$\bar\Omega_{\rm k0}$		Bare curvature parameter
$\bar\Omega_{\mathcal{Q}0}$		Bare backreaction parameter
$\bar z_{\rm dec}$		Bare redshift of decoupling
$\bar z_{\rm drag}$		Bare redshift of drag epoch
$\bar D_{\rm s}(\bar z_{\rm dec})$		proper size of sound horizon at $\bar z = \bar z_{\rm dec}$ (Mpc)
$\bar D_{\rm s}(\bar z_{\rm drag})$		proper size of sound horizon at $\bar z = \bar z_{\rm drag}$ (Mpc)
$\tau_{\rm w0}$		Age of the Universe (galaxy/ wall observer in Gyr)
$\Omega_{\rm B0}$		Dressed baryon density parameter
$\Omega_{\rm C0}$		Dressed cold dark matter density parameter
$\Omega_{\rm M0}$		Dressed total matter density parameter
$z_{\rm dec}$		Dressed redshift of decoupling
$z_{\rm drag}$		Dressed redshift of drag epoch
$100\theta_{\rm dec}$		$100\times$ angular scale of sound horizon at $z = \bar z_{\rm dec}$
$100\theta_{\rm drag}$		$100\times$ angular scale of sound horizon at $z = \bar z_{\rm drag}$
$d_{\rm A}$		Dressed angular diameter distance to sound horizon at decoupling (Mpc)
$d_{\rm A,drag}$		Dressed angular diameter distance to sound horizon at drag epoch (Mpc)

the lensed temperature power spectrum with reionization turned on for the timescape matched FLRW model. We assume the reionization optical depth $\tau_{\rm rion}$ to be completely degenerate with $A_{\rm s}$.

D. Choice of matched FLRW models

Many of the matching methods of Sec. III C require a shift (4) of very large ℓ multipoles of equivalent FLRW models with large spatial curvatures of order $0.2 \lesssim \hat\Omega_{\rm k0} \lesssim 0.8$. In these cases the amount of time required to solve the Boltzmann code becomes prohibitively large in combination with the MCMC analysis. We checked that individual runs of the A($\bar r_{\mathcal{H}}$), A($\bar\eta_0$), A(t_0) and A($\hat\Omega_{\Lambda 0} = 0$) matched models gave similar χ^2 values to the canonical A($\bar H_{\rm dec}$) matched model, but were unable to determine best fit parameter values with the computing resources available. Our MCMC analysis is therefore restricted to matched models A($\bar H_{\rm dec}$), W($k = 0$) and W($k \neq 0$).

The wall geometry matching methods W($k = 0$) and W($k \neq 0$) cannot give as good a fit as the canonical A($\bar H_{\rm dec}$) method to the volume–average expansion history. However, they may provide better matching for those aspects of the power spectra which are independent of the distance to the surface of last scattering. Consequently, differences between the two methodologies also provide a measure of the systematic uncertainties inherent in our matched FLRW model approach.

E. Foreground modeling

Foregrounds can bias estimation of cosmological parameters, a problem which is not unique to our study but also besets all analyses of CMB data sets in the context of FLRW models as well. The `CamSpec` likelihood in the $50 \leq \ell \leq 2500$ multipole range takes 14 additional parameters that are used for relative calibration and unresolved foreground modeling. The Planck team[8] find that foreground modeling does not change the parameter constraints in their baseline six-parameter ΛCDM model $\{\Omega_{\rm b}h^2,\ \Omega_{\rm c}h^2,\ 100\theta_{\rm MC},\ \tau,\ n_{\rm s},\ \ln(10^{10}A_{\rm s})\}$. However, they find that extensions to their baseline model are sensitive to foreground modeling with the independent likelihood code `Plik` converging to slightly different values of $Y_{\rm p}$, $N_{\rm eff}$, $n_{\rm s}$. They report up to a 1σ shift in parameter values from the two likelihood codes in some cases, but manage to obtain better agreement with the inclusion of high–ℓ data which constrain the foregrounds to a higher precision.

We have investigated the possibility that foreground modeling may critically impact the timescape parameter constraints. As a test we fixed the foreground nuisance parameters to the best fit baseline ΛCDM model values from Planck [71], with the hypothesis that the baseline ΛCDM model unambiguously identifies the foreground sources and their impact on the temperature power spectrum. Fixing the foreground parameters in this way we found the best fit parameters for the timescape cosmology to be $f_{\rm v0} = 0.607^{+0.051}_{-0.057}$, $H_0 = 59.72^{+2.76}_{-2.89}\,{\rm km\ sec^{-1}\,Mpc^{-1}}$, $10^{10}\eta_{B\gamma} = 6.24^{+0.3}_{-0.29}$, $n_{\rm s} = 0.971^{+0.028}_{-0.030}$ (using the canonical $\mathrm{A}(\bar{H}_{\rm dec})$ matched model). Thus the chains converged to roughly the same region in parameter space, the best fit parameters being within the 1σ constraints from Table II, but with a larger value of $-\ln\mathcal{L} = \chi^2/2$ as compared with the case in which foreground model nuisance parameters are free to vary. These results are therefore consistent with the hypothesis that foregrounds do not have a critical impact on parameter estimation.

The precise value of the goodness of fit, $-\ln\mathcal{L} = \chi^2/2$, obtained with fixed foreground nuisance parameters is not of acute importance since we only use the Planck data, and do not combine it with other data sets. If we were to combine the Planck data with other data sets that constrain the CMB anisotropy spectrum, the issues around foreground modeling would need to be revisited.

While we cannot entirely rule out the impact of foreground modeling on timescape parameters we proceed with the assumption that our results are not critically impacted by them. We treat the 14 foreground parameters of the baseline model as nuisance parameters and adopt the same prior range for these parameters as for the baseline ΛCDM model in the analysis by the Planck team [71].

[8] See Sec. 4.2 and Appendix C in [71].

V. RESULTS AND ANALYSIS

Here we present the parameter constraints obtained from the Planck temperature power spectrum data in the range $50 \leq \ell \leq 2500$. Our analysis includes the parameters that model the foreground in this multipole range [71].

In Table II we record the best fit and mean marginalized constraints on timescape parameters obtained for each of the matching procedures $\mathrm{A}(\bar{H}_{\rm dec})$, $\mathrm{W}(k=0)$ and $\mathrm{W}(k\neq 0)$ with $N_{\rm eff} = 3.046$ fixed. The chains analyses and all statistical information were obtained with the `getdist` software in the CosmoMc package [59]. We ran eight chains for the canonical $\mathrm{A}(\bar{H}_{\rm dec})$ matching method and five chains each for the $\mathrm{W}(k=0)$ and $\mathrm{W}(k\neq 0)$ methods. We have checked to ensure that the base MCMC parameters satisfy the Gelman–Rubin[9] diagnostic $R-1 < 0.01$ and that the chains have converged. Not all of the derived parameters satisfy these criteria but even then all parameters satisfy $R-1<0.02$ and are in fact closer to 0.01 than to 0.02.

In what follows we treat the $\mathrm{A}(\bar{H}_{\rm dec})$ model as the canonical matching procedure and its results will be used for timescape parameter constraints. The other matching procedures are used for the purpose of understanding the effects of matching assumptions on parameter constraints and possible systematic uncertainties.

In Fig. 7 the marginalized probability distribution and 2–dimensional posterior constraints for the base timescape parameters and the dressed total matter density are shown for the canonical $\mathrm{A}(\bar{H}_{\rm dec})$ matching. The constraints on all parameters can be understood in terms of the angular scale of the sound horizon $\theta_{\rm dec} = \bar{D}_{\rm s}(\bar{z}_{\rm dec})/d_{\rm A}$ and the ratios of the acoustic peaks.

Before proceeding any further let us first make the relationship between $\Omega_{\rm M0}$ and $f_{\rm v0}$ conspicuous. At late epochs the full timescape solution with radiation is very well approximated by the tracker limit of the matter only solution [2], leading to the following relations between the present void fraction and dressed matter density

$$\Omega_{\rm M0} \approx \tfrac{1}{2}\,(1-f_{\rm v0})\,(2+f_{\rm v0})\ , \quad \left.\frac{{\rm d}\Omega_{\rm M}}{{\rm d}f_{\rm v}}\right|_0 \approx -\left(\tfrac{1}{2}+f_{\rm v0}\right), \tag{63}$$

which explains the negative correlation between $\Omega_{\rm M0}$ and $f_{\rm v0}$. The Planck data tightly constrain the angular posi-

[9] The Gelman–Rubin diagnostic is used to test that all chains converge to the same posterior distribution [75]. The $R-1$ statistic in the diagnostic compares the variance of the chain means to the mean value of the variances within each chain. Generally $R-1<0.2$ is optimal but even then low values indicate, but do not guarantee, convergence.

TABLE II: The best fit and mean timescape parameter values, with 68% uncertainties. A fixed $N_{\rm eff} = 3.046$ is assumed. The timescape models are matched to FLRW models with the same expansion history until recombination up to density parameter differences of $< 10^{-4}$. We show only those matching methods for which the matched FLRW curvature parameter is small enough to permit a full MCMC analysis using available computer resources. The A($\bar{H}_{\rm dec}$) average expansion history matching method provides the canonical constraint on timescape parameters. The wall expansion history matching methods, W($k = 0$) and W($k \neq 0$), are computed for illustrative purposes.

Matching type		A($\bar{H}_{\rm dec}$)		W($k = 0$)		W($k \neq 0$)
Parameter	Best fit	Mean (68% limits)	Best fit	Mean (68% limits)	Best fit	Mean (68% limits)
$f_{\rm v0}$	0.628	$0.627^{+0.014}_{-0.012}$	0.545	$0.550^{+0.017}_{-0.015}$	0.559	$0.557^{+0.017}_{-0.015}$
H_0	60.984	$60.997^{+0.791}_{-0.733}$	56.148	$56.364^{+0.700}_{-0.694}$	56.774	$56.710^{+0.707}_{-0.714}$
$10^{10}\eta_{B\gamma}$	6.465	$6.489^{+0.101}_{-0.102}$	6.043	$6.048^{+0.086}_{-0.087}$	6.080	$6.080^{+0.091}_{-0.089}$
$n_{\rm s}$	0.995	0.992 ± 0.009	0.956	0.957 ± 0.009	0.963	0.960 ± 0.009
$\bar{H}_0$	51.640	$51.658^{+0.251}_{-0.257}$	49.846	$49.882^{+0.223}_{-0.218}$	50.016	$49.996^{+0.227}_{-0.225}$
$\bar{T}_0$	2.074	2.074 ± 0.010	2.142	2.137 ± 0.013	2.130	2.131 ± 0.013
t_0	16.587	16.579 ± 0.042	16.640	$16.664^{+0.056}_{-0.054}$	16.675	$16.671^{+0.058}_{-0.053}$
$\bar{\gamma}_0$	1.314	1.314 ± 0.007	1.273	1.275 ± 0.008	1.280	1.279 ± 0.008
$Y_{\rm p}$	0.248	0.248 ± 0.00015	0.247	0.247 ± 0.00014	0.247	0.247 ± 0.00014
$\bar{\Omega}_{\rm B0}$	0.039	0.039 ± 0.001	0.043	0.043 ± 0.001	0.042	0.043 ± 0.001
$\bar{\Omega}_{\rm C0}$	0.176	$0.176^{+0.008}_{-0.010}$	0.238	$0.234^{+0.012}_{-0.013}$	0.227	$0.228^{+0.012}_{-0.013}$
$\bar{\Omega}_{\rm M0}$	0.215	$0.216^{+0.009}_{-0.011}$	0.281	$0.277^{+0.012}_{-0.014}$	0.269	$0.271^{+0.012}_{-0.014}$
$\bar{\Omega}_{\rm k0}$	0.819	$0.818^{+0.010}_{-0.008}$	0.757	$0.762^{+0.013}_{-0.012}$	0.768	$0.767^{+0.013}_{-0.011}$
$\bar{\Omega}_{\mathcal{Q}0}$	-0.034	-0.034 ± 0.001	-0.038	-0.038 ± 0.001	-0.038	-0.038 ± 0.001
$\bar{z}_{\rm dec}$	1429.729	$1429.425^{+7.171}_{-6.165}$	1387.674	$1390.524^{+8.570}_{-7.723}$	1394.902	$1394.064^{+8.473}_{-7.723}$
$\bar{z}_{\rm drag}$	1396.292	$1396.341^{+8.081}_{-6.996}$	1348.949	$1351.776^{+9.231}_{-8.309}$	1356.537	$1355.719^{+8.522}_{-8.515}$
$\bar{D}_{\rm s}(\bar{z}_{\rm dec})$	0.135	0.135 ± 0.001	0.132	0.132 ± 0.001	0.133	0.133 ± 0.001
$\bar{D}_{\rm s}(\bar{z}_{\rm drag})$	0.140	0.140 ± 0.001	0.139	0.139 ± 0.001	0.139	0.139 ± 0.001
$\tau_{\rm w0}$	13.811	$13.806^{+0.067}_{-0.065}$	14.267	$14.261^{+0.058}_{-0.052}$	14.229	$14.233^{+0.059}_{-0.054}$
$\Omega_{\rm B0}$	0.089	0.089 ± 0.001	0.089	0.089 ± 0.001	0.089	0.089 ± 0.001
$\Omega_{\rm C0}$	0.400	$0.400^{+0.014}_{-0.016}$	0.490	0.484 ± 0.017	0.475	0.477 ± 0.017
$\Omega_{\rm M0}$	0.489	$0.489^{+0.014}_{-0.016}$	0.579	0.573 ± 0.017	0.564	0.566 ± 0.017
$z_{\rm dec}$	1087.568	$1087.503^{+0.480}_{-0.520}$	1090.141	$1090.039^{+0.494}_{-0.495}$	1089.800	$1089.822^{+0.498}_{-0.507}$
$z_{\rm drag}$	1062.128	$1062.323^{+0.723}_{-0.732}$	1059.713	$1059.655^{+0.638}_{-0.646}$	1059.820	$1059.836^{+0.666}_{-0.667}$
$100\,\theta_{\rm dec}$	1.048	1.047 ± 0.001	1.041	1.041 ± 0.001	1.041	1.041 ± 0.001
$100\,\theta_{\rm drag}$	1.064	1.064 ± 0.001	1.061	1.061 ± 0.001	1.061	1.061 ± 0.001
$d_{\rm A}$	12.888	12.883 ± 0.063	12.699	$12.729^{+0.067}_{-0.066}$	12.753	$12.750^{+0.067}_{-0.066}$
$d_{\rm A,drag}$	13.191	13.183 ± 0.062	13.058	$13.088^{+0.066}_{-0.065}$	13.108	$13.104^{+0.067}_{-0.066}$

tion of the first peak, $\theta_{\rm dec}$, and therefore any changes in H_0, $\Omega_{\rm M0}$, $f_{\rm v0}$ which lead to an increase in $d_{\rm A}$ simultaneously result in an increase in $\bar{D}_{\rm s}$ and vice versa. A larger angular diameter distance, d_A, to the last scattering surface can be obtained by increasing either H_0 or $f_{\rm v0}$ but there is a concurrent increase in $\bar{D}_{\rm s}$, which also changes the ratios of the acoustic peak heights.

Matching the ratios of the peak heights requires a delicate balance between the proportions of baryonic and nonbaryonic matter. The extent to which $f_{\rm v0}$ can change while keeping $\theta_{\rm dec}$ constant is limited because the ratio $\Omega_{\rm M0}/\Omega_{\rm B0}$ (or equivalently $f_{\rm v0}/\eta_{B\gamma}$) fixes the ratios of the first, second and third acoustic peak heights, which are

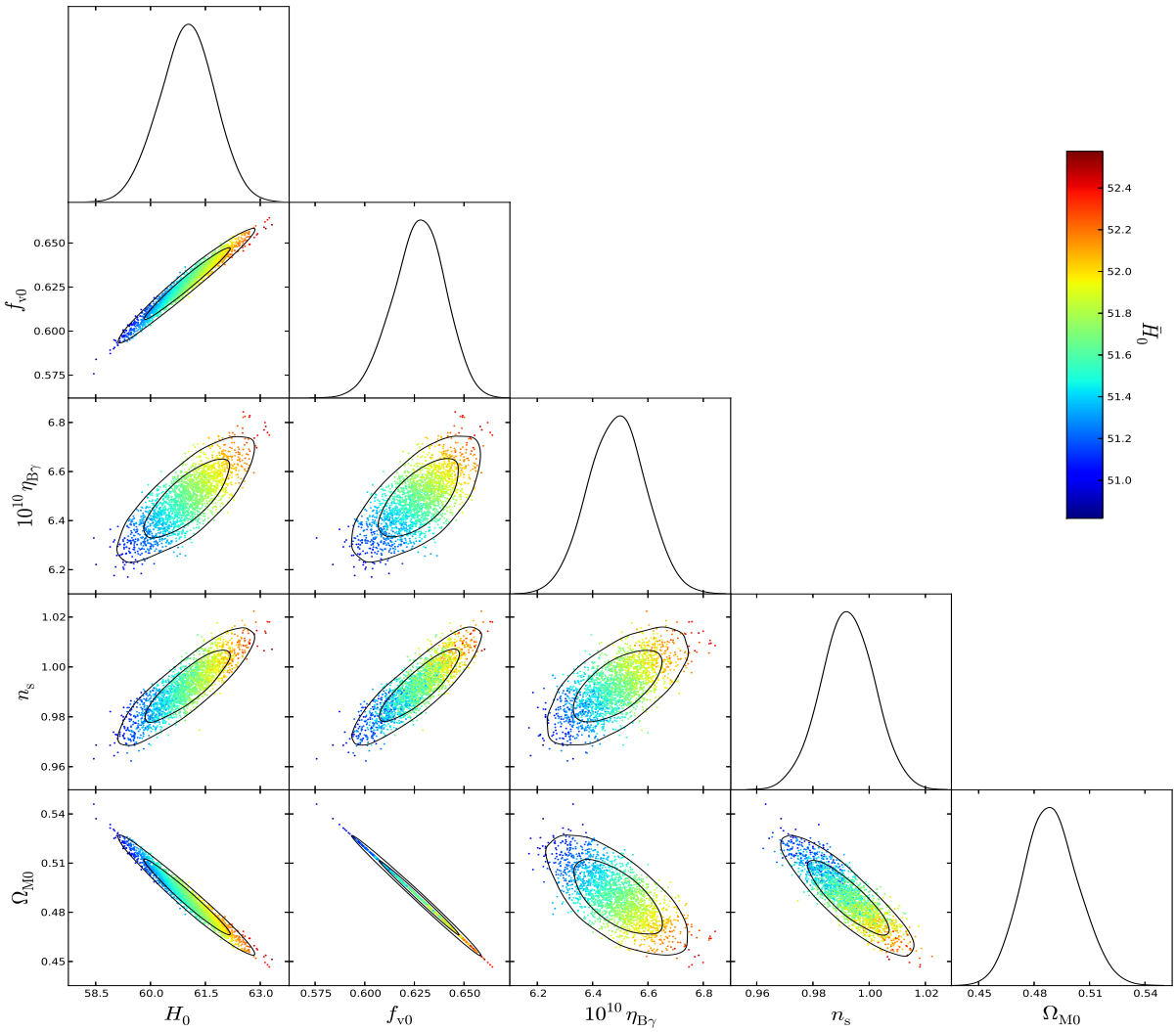

FIG. 7: Constraints on the base MCMC parameters for the timescape parameters listed in Table I, and the total dressed matter density, $\Omega_{\rm M0}$ for timescape parameters with matched model A($\bar{H}_{\rm dec}$), showing 68% and 95% statistical uncertainties. We also show a scatter plot of the parameters colour coded with the value of the bare Hubble constant, $\bar{H}_0$, relevant to a volume–average expansion.

also tightly constrained by the Planck data.

In the FLRW models one of the two parameters, $\Omega_{\rm k0}$ and $\Omega_{\Lambda 0}$ (as constrained from the Friedman equation) can be adjusted to determine the overall angular scale of the peaks without directly influencing the ratios of the acoustic peak heights. By contrast, in the timescape model the void fraction constrains both the matter density parameter – either dressed (63) or bare $\bar{\Omega}_{\rm M0} \approx 4(1-f_{\rm v0})/(2+f_{\rm v0})^2$ – and the volume average curvature density parameter, $\bar{\Omega}_{\rm k0} \approx 9 f_{\rm v0}/\left(2+f_{\rm v0}\right)^2$. Thus timescape parameters are very tightly constrained; a change to $f_{\rm v0}$ can significantly affect both the angular scale and, insofar as it changes the ratio $\Omega_{\rm B0}/\Omega_{\rm M0}$, also the ratios of the peak heights.

The results of MCMC analysis on the canonical A($\bar{H}_{\rm dec}$) model yield $H_0 = 61.0^{+0.79}_{-0.73}\,{\rm km\ sec^{-1}\,Mpc^{-1}}$ and $f_{\rm v0} = 0.627^{+0.014}_{-0.012}$. The value of the dressed Hubble constant agrees with our previous estimate, $61.7 \pm 3.0\,{\rm km\ sec^{-1}\,Mpc^{-1}}$ [8] at the 1σ level. However, the void fraction is almost 2σ less than the previous estimate [8], $f_{\rm v0} = 0.695^{+0.041}_{-0.051}$. Of course, we should caution that the uncertainties given in Table II do not include any estimate of the systematic uncertainties that must surely arise from the matched FLRW procedure. Since the wall geometry based matching procedures W($k=0$) and W($k\neq 0$) do not reliably estimate volume average quantities[10], the significantly smaller values of H_0, $f_{\rm v0}$

[10] The present epoch values of the void fraction for the W($k=0$)

obtained for these procedures probably overestimate the systematic uncertainties. However, as an upper bound they indicate that the systematic uncertainties could be as high as 8–13%, as compared to the 1–2% statistical uncertainties.

Even if the systematic uncertainties were not so large, however, there is an obvious reason for the apparent tension between the two estimates of $f_{\rm v0}$. In all previous work [1, 5, 8] we have not directly constrained the baryon–to–photon ratio. In fact, our best previous estimate [8] is based on assuming a baryon–to–photon ratio $10^{10}\eta_{B\gamma} = 5.1 \pm 0.5$ for which one can avoid a primordial lithium abundance anomaly [52, 53]. By contrast, here we have used the acoustic peaks height ratio to directly constrain $\eta_{B\gamma}$ for the first time, with the result $10^{10}\eta_{B\gamma} = 6.49 \pm 0.10$. If we had admitted such large values of the baryon–to–photon ratio in our previous estimate then there would not be a discrepancy.

We find that while the timescape model remains observationally consistent a detailed analysis of the acoustic peaks in the Planck data – modulo systematic uncertainties introduced by the model matching procedure – the baryon–to–photon ratio is driven to a value that is even higher than ΛCDM model estimates [71, 76]. Thus based on the analysis here we cannot make the claim that the timescape model solves the primordial lithium abundance anomaly.

One might be concerned that the value of the baryon–to–photon ratio is $4\,\sigma$ larger than the ΛCDM value $10^{10}\eta_{B\gamma} = 6.04 \pm 0.09$. However, the wall geometry based matching procedures give values $10^{10}\eta_{B\gamma} = 6.05 \pm 0.09$ and $10^{10}\eta_{B\gamma} = 6.08 \pm 0.09$, which precisely match the ΛCDM result. Considering the systematic uncertainties therefore, we have agreement with ΛCDM.

The spectral index is also constrained for the first time. The canonical $\mathrm{A}(\bar{H}_{\rm dec})$ matching method leads to a nearly scale invariant primordial spectrum with $n_{\rm s} = 0.992 \pm 0.009$, $n_{\rm s} = 0.960 \pm 0.009$ whereas the wall–geometry matching methods yield $n_{\rm s} = 0.957 \pm 0.009$ and $n_{\rm s} = 0.960 \pm 0.009$, confirming deviations from scale invariance at more than $3\,\sigma$ level in agreement with the ΛCDM results [71, 76]. Once again, these 3–4% differences are driven by the systematic uncertainties that arise from the imperfect nature of the matched model procedures.

Since $10^{10}\eta_{B\gamma}$ and $n_{\rm s}$ constrain spectral features other than the overall angular scale, the difference between the average–geometry and wall–geometry matching procedures give a reasonable estimate of the systematic uncertainties. In fact, the the wall–geometry matching procedures produce a somewhat reduced value of $-\ln\mathcal{L} = \chi^2/2$ as compared to the volume–average methods, with $-\ln\mathcal{L} = 3925.16$, 3897.90 and 3896.47 for the $\mathrm{A}(\bar{H}_{\rm dec})$, $\mathrm{W}(k=0)$ and $\mathrm{W}(k\neq 0)$ methods respectively. The likelihoods for the $\mathrm{W}(k=0)$, $\mathrm{W}(k\neq 0)$ matching methods are in fact precisely the same as one obtains for best fit ΛCDM model in the multipole range $50 \leq \ell \leq 2500$, where the Planck team obtain [77] $-\ln\mathcal{L} = 3895.5$ using `MINUIT` or $-\ln\mathcal{L} = 3896.9$ using `CosmoMC`.

It therefore appears that the FLRW perturbation theory for the wall–geometry matching methods produces a better fit to the features of the acoustic peaks which relate solely to its shape. It is possible that the values of $10^{10}\eta_{B\gamma}$ and $n_{\rm s}$ obtained by wall geometry matching therefore give a more accurate estimate of the values that we would obtain if we could both use the most relevant perturbation equations, and simultaneously use the timescape solution in all of the codes, rather than having to rely on matched models using CLASS [55, 56].

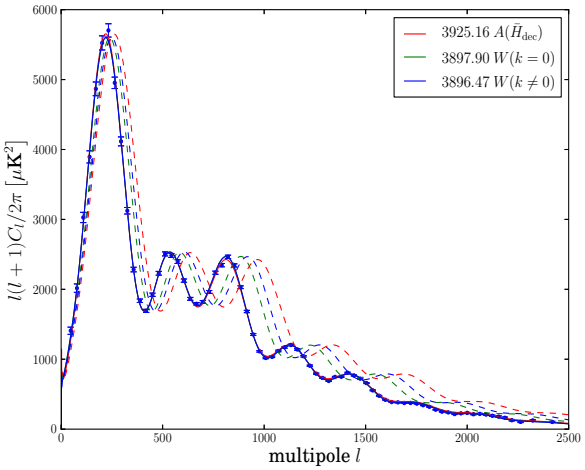

FIG. 8: Angular power spectra for the best fit parameters of the three matching methods $\mathrm{A}(\bar{H}_{\rm dec})$ (red); $\mathrm{W}(k=0)$ (green); $\mathrm{W}(k\neq 0)$ (blue), with $-\ln\mathcal{L}$ values shown. In each case the dashed lines show the spectrum before the application of the shift (4), and the solid lines after. Data points, plotted for $\ell \geq 50$, are derived from the `CAMspec` likelihood [71], with $1\,\sigma$ error bars including beam and foreground uncertainties.

In Fig. 8 the power spectra for the best fit values are shown for the three matching procedures for which the MCMC analysis was possible. To show the level of concurrence of the other volume–average expansion history matching procedures from Sec. III C, we determined their power spectra using the best fit parameters for $\mathrm{A}(\bar{H}_{\rm dec})$ matching found by the MCMC analysis. In Fig. 9 we plot the ratios of these power spectra relative to a fiducial ΛCDM spectrum obtained from the best fit parameters using the Planck data only [71]. We also plot the same ratio for the three best fit models of Table II.

We see in Fig. 9 that the difference in individual

and $\mathrm{W}(k\neq 0)$ methods listed in Table II have $f_{\rm v0} < 0.587$ and thus represent models with no apparent cosmic acceleration [1, 2], whereas the $\mathrm{A}(\bar{H}_{\rm dec})$ matched model does have apparent acceleration

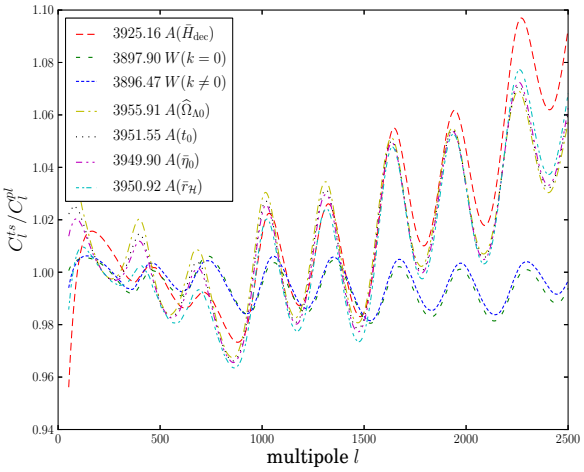

FIG. 9: Ratios of multipoles of matched timescape models to those of the ΛCDM model with the best fit Planck parameters, which is used as a reference model. For the A($\bar{H}_{\rm dec}$), W($k=0$) and W($k\neq 0$) methods the best fit values from Table II have been used. For the A($\bar{r}_{\mathcal{H}}$), A($\bar{\eta}_0$), A(t_0) and A($\hat{\Omega}_{\Lambda 0}=0$) we have used the best fit parameters from the A($\bar{H}_{\rm dec}$) model. The values of $-\ln\mathcal{L}=\chi^2/2$ shown do not therefore represent the best fit values in these cases.

C_ℓ values from the ΛCDM model is of up to order 1% for the wall expansion history matching methods over all multipoles. For the volume–average matching methods the differences are individually up to 2–3% for $50\lesssim\ell\lesssim 1600$, and slowly rise to a maximum $\sim$8–9% for $2300\lesssim\ell\lesssim 2500$. While the small angle differences may seem large, it must be remembered that individual foreground parameters will also be somewhat different so that the overall $(-\ln\mathcal{L})$ value for the best fit A($\bar{H}_{\rm dec}$) matched model is only 0.7% larger than for the best fit ΛCDM model [71].

We note that in Fig. 9 the increased power in the canonical A($\bar{H}_{\rm dec}$) matching method as compared to the fiducial ΛCDM power spectrum at very large multipoles will be partly due to the difference in spectral index $n_{\rm s}=0.992\pm 0.009$ compared to $n_{\rm s}=0.9616\pm 0.0094$. Increasing $n_{\rm s}$ increases the power at the third peak and higher multipoles (small angles) compared to the first two peaks [35].

In Figs. 10 and 11 the posterior constraints on the dressed and bare parameters are shown against the base MCMC parameters. These figures illustrate a number of interesting points relating to the constraints $\eta_{B\gamma}$ and $n_{\rm s}$. In Fig. 11 the bare baryon density $\bar{\Omega}_{\rm B0}$ appears to be uncorrelated to $\eta_{B\gamma}$. Thus since $\eta_{B\gamma}\propto\bar{\Omega}_{\rm B0}\bar{H}_0^2$, any increase in $\eta_{B\gamma}$ must be met with an increase in $\bar{H}_0$. By contrast, the dressed baryon density parameter, $\Omega_{\rm B0}$ is positively correlated with $\eta_{B\gamma}$, as shown in Fig. 10. The phenomenological lapse function, $\bar{\gamma}$, and its time derivative, $d\bar{\gamma}/dt$, which relate the dressed and bare parameters according to $\Omega_{\rm B0}=\bar{\Omega}_{\rm B0}/\bar{\gamma}_0^3$ and $H_0=(\bar{\gamma}\bar{H}-d\bar{\gamma}/dt)\big|_0$, are involved here in subtle ways which are difficult to disentangle. This also explains why the volume–average geometry and wall–geometry matching methods lead to different results for $\eta_{B\gamma}$. Essentially, one cannot separate parameters concerning the average expansion history from those that relate to spectral features such as the ratios of acoustic peak heights.

The variation in the spectral index, $n_{\rm s}$, between the different matching methods can be similarly understood. Figures 10 and 11 reveal a degeneracy between $n_{\rm s}$ and the dressed and bare parameters $\Omega_{\rm M0}$, $\bar{\Omega}_{\rm M0}$, $\Omega_{\rm B0}$, $\bar{H}_0$. One cannot disassociate the early universe physics which is influenced by $n_{\rm s}$ from the late time evolution on account of parameter degeneracies. The lesson here is that, as yet, the constraints on the timescape parameters are limited by systematic uncertainties from the matching method which are larger than the statistical uncertainties. Furthermore, the exclusion of $\ell<50$ data is also a handicap for us since the Sachs–Wolfe plateau on the largest scales is sensitive to $n_{\rm s}$, where the largest wavelengths remain frozen outside the horizon before recombination and are unaffected by causal physics.

In Fig. 12 the correlations between the derived bare and dressed parameters are shown. The narrow 68% and 95% confidence contours between various parameters largely reinforce what we already know about their degeneracies from the timescape matter–only tracker solution [2, 3]. In the limit of vanishing radiation energy density the width of the contours would shrink to zero. The 2–dimensional posteriors involving baryon density are not as tightly constrained because the tracker solution fixes the total matter density but not its split into baryonic and nonbaryonic components. Interpreting H_0 as the Hubble constant determined by wall observers, and $\bar{H}_0$ as the Hubble constant of the volume–average statistical geometry, the contours in the H_0 – $\bar{H}_0$ plane in Fig. 12 show that bounds on the bare parameter provide reasonably tight bounds on the dressed parameter and vice versa.

Finally, in Fig. 13 the marginalized likelihoods for all the timescape parameters of the canonical matching listed in Table I are shown for completeness.

Among the derived parameters in Table II, it is interesting to note that the age of the Universe as measured by a wall observer, $\tau_{\rm w0}=13.81\pm 0.07$ Gyr, matches the standard ΛCDM fit to Planck [71]. It should be stressed that this numerical result is not at all related to the matched ΛCDM model, which for the A($\bar{H}_{\rm dec}$) method in the best fit case has $\hat{\Omega}_{\Lambda 0}=0.7633$, $\hat{\Omega}_{\rm M0}=0.2153$, $\hat{\Omega}_{\rm k0}=0.02138$ and a matched age of 19.81 Gyr in volume–average time. Wall geometry matching gives $\tau_{\rm w0}=14.26\pm 0.06$ Gyr and $\tau_{\rm w0}=14.23\pm 0.06$ Gyr for the W($k=0$) and W($k\neq 0$) methods respectively, once again indicating that the systematic uncertainties are larger than the statistical uncertainties, being of order 3.5% in this case.

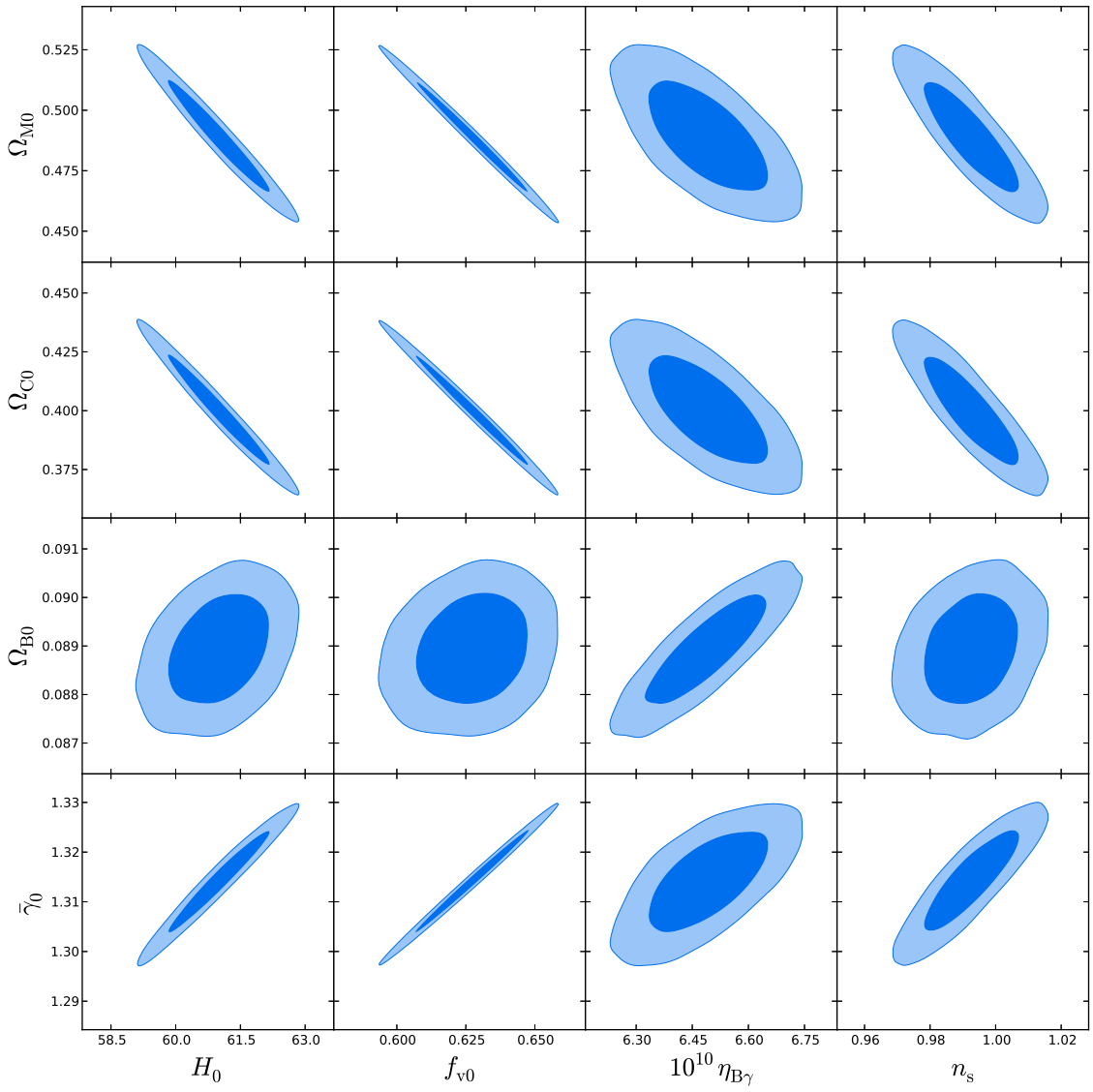

FIG. 10: Variations in the various dressed parameters are shown with respect to the base MCMC parameters for the timescape model. The parameter constraints – showing 68% and 95% statistical uncertainties – are determined for the case of the A($\bar{H}_{\rm dec}$) matching method.

The present comoving scale of the baryon acoustic oscillation, which is given by

$$r_{\rm drag} = (1 + z_{\rm drag})\theta_{\rm drag} d_{\rm A,drag} \qquad (64)$$

is determined by the parameters of Table II to be $r_{\rm drag} = 149.3 \pm 0.7\,$Mpc for the canonical A($\bar{H}_{\rm dec}$) matched model, and $r_{\rm drag} = 147.0 \pm 0.7\,$Mpc and $r_{\rm drag} = 147.5 \pm 0.7\,$Mpc for the W($k = 0$) and W($k \neq 0$) methods respectively. The systematic uncertainties between the different methods, of order 1.5%, are smaller than for other parameters. In this case the W($k = 0$) and W($k \neq 0$) values precisely match the ΛCDM best fit value from Planck, $r_{\rm drag} = 147.34\,$Mpc.

VI. DISCUSSION

We have for the first time investigated the parameter bounds that can be put on the timescape cosmology through a full analysis of the acoustic peaks in the power spectrum of CMB anisotropies, using Planck satellite data. Since the expansion history of the timescape model differs only slightly from that of a FLRW model at early epochs, we performed our analysis by directly computing relevant processes (such as nucleosynthesis and recombination) for the timescape model in the early Universe, and then matched the expansion history of the timescape model to that of the closest equivalent FLRW model in volume–average coordinates. We investigated

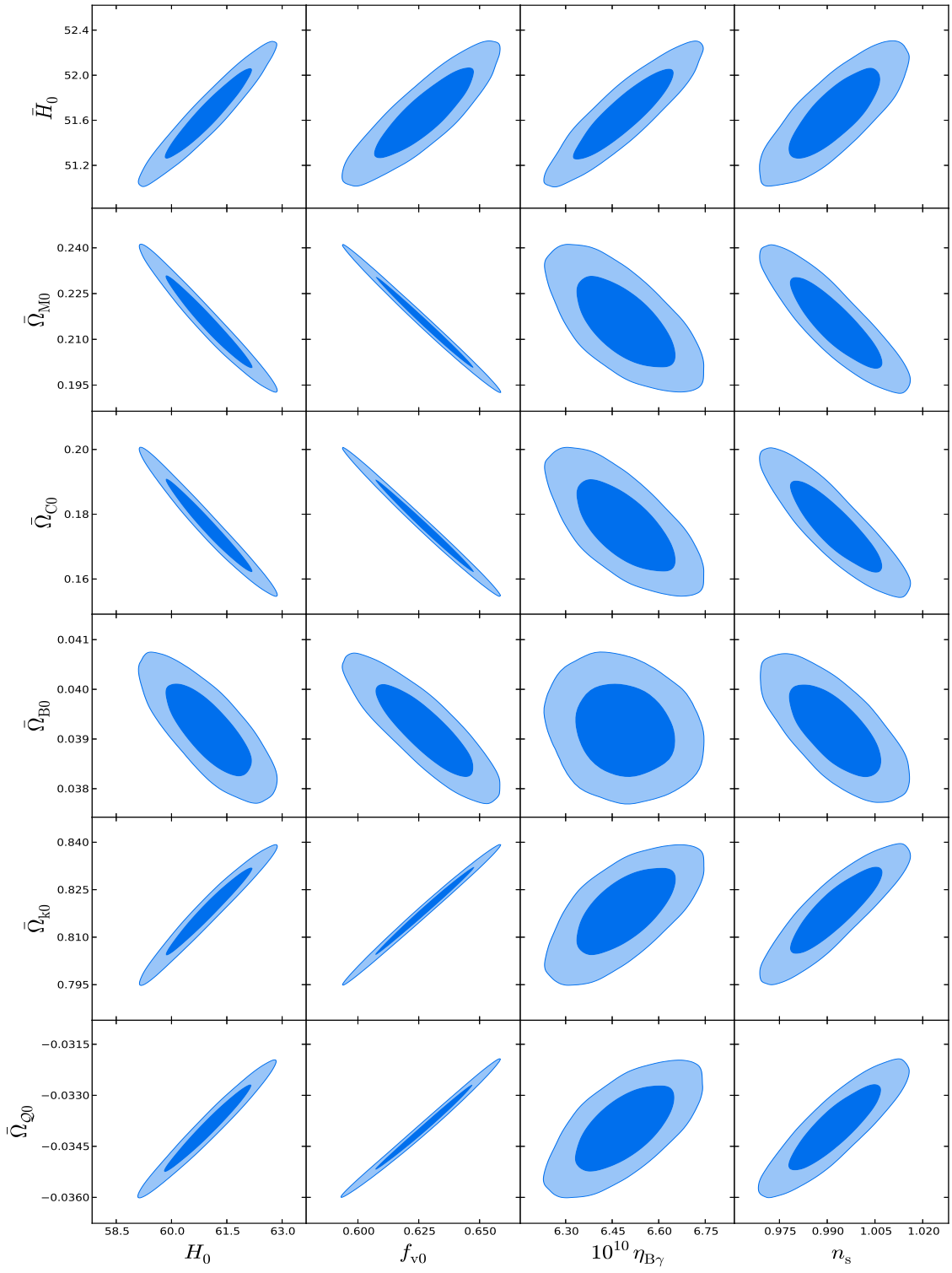

FIG. 11: Variations in the various bare parameters are shown with respect to the base MCMC parameters for the timescape model. The parameter constraints – showing 68% and 95% statistical uncertainties – are determined for the case of the A($\bar{H}_{\rm dec}$) matching method.

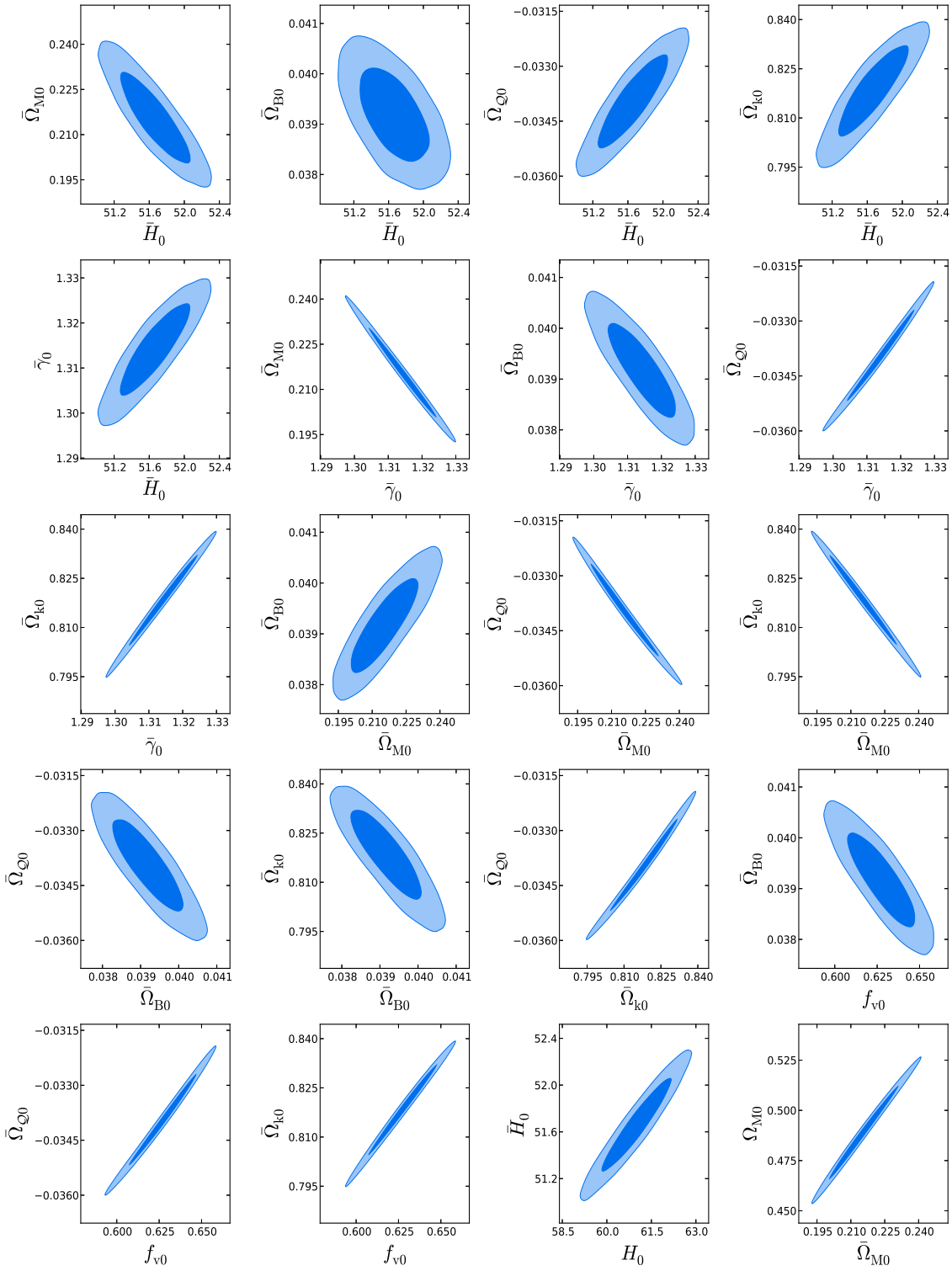

FIG. 12: Correlations between selected bare and dressed timescape parameters are shown. The parameter constraints – showing 68% and 95% statistical uncertainties – are determined for the case of the A($\bar{H}_{\rm dec}$) matching method.

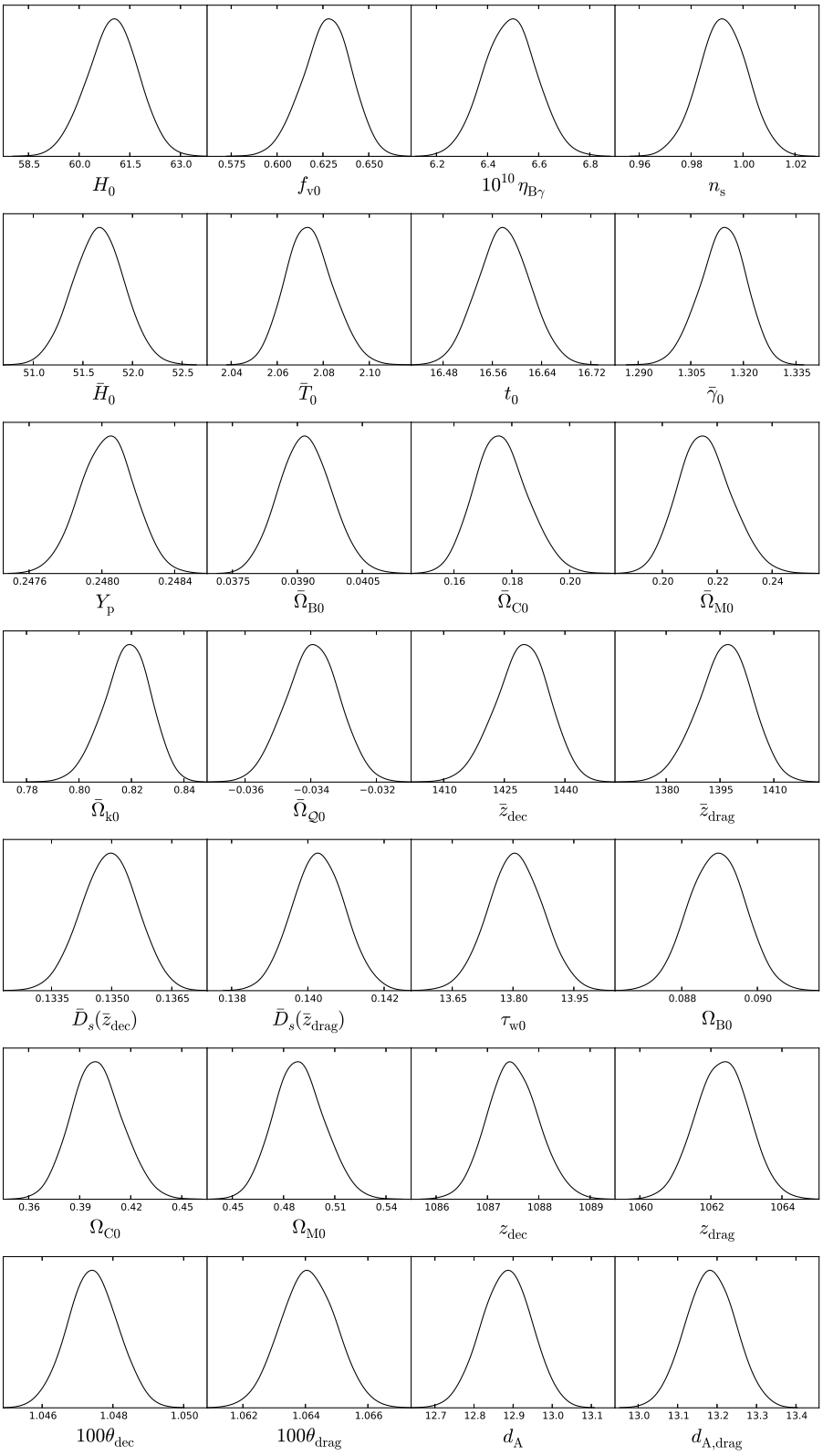

FIG. 13: Marginalized posteriors for the base MCMC parameters, the bare parameters and the dressed parameters in the timescape cosmology. The parameter constraints are determined for the case of the A($\bar{H}_{\rm dec}$) matching method.

a number of matching procedures, but used the $\mathrm{A}(\bar{H}_{\mathrm{dec}})$ matching to provide statistical bounds on parameters related to the average expansion history.

We conclude that there are parameters for which the timescape model is a good fit to the Planck data, and it remains competitive with the ΛCDM model. However, we can no longer claim a resolution of the primordial lithium abundance problem, as seemed possible with fits based solely on the angular diameter distance of the sound horizon at decoupling and the baryon drag epoch [8]. This is our most important result.

It is clear, however, that this conclusion is driven by the ratio of the heights of the acoustic peaks which depend strongly on the ratio of baryons to nonbaryonic dark matter in the primordial plasma. Furthermore, these results depend heavily on perturbation theory in the early Universe for which a standard ΛCDM model has been assumed, with possibly different constituent ratios.

Although backreaction is negligible in determining the background solution, in our numerical examples $\bar{\Omega}_{\mathcal{Q}\,\mathrm{dec}} \sim -1 \times 10^{-5}$ is of the same order as the density perturbations, $\delta\rho/\rho$, in baryons at decoupling. Thus although the backreaction terms are inconsequential in determining the background at early times they very probably should *not* be neglected in considering the evolution of perturbations in determining the acoustic peaks. By analogy, in the standard treatment both density and velocity perturbations are small and do not significantly affect the background but being of similar order they must be considered as a coupled system. The fact that different matched FLRW model procedures give rise to systematic uncertainties of 8–13% in some present epoch parameters, is a direct demonstration that differences of order 10^{-5} between the matched models at decoupling are nonetheless significant.

Ideally therefore we should consider the backreaction formalism with pressure [31] for a matter plus radiation plasma which begins in close to homogeneous and isotropic state. Since the average evolution is not *exactly* a Friedmann model, such an analysis is subtly different from a perturbative approach which assumes that average evolution is exactly a solution of Einstein's equations. The problem of backreaction in the primordial plasma has not been studied in any more detail than Buchert's initial formal study [31]. There is much discussion of backreaction in models which are close to FLRW backgrounds, but debate has centred on the question of whether backreaction can cause significant deviations of the average evolution from FLRW evolution in the case of dust cosmologies [27]. The question here differs both by the virtue of the matter content, and by the fact that we are interested in changes to the growth of perturbations rather than the average evolution itself. As far as physical cosmology is concerned, this is completely uncharted territory.

To summarize our results, if we take the canonical $\mathrm{A}(\bar{H}_{\mathrm{dec}})$ matching method to estimate the parameters which describe the average expansion history, but use the difference in the wall geometry matching method results of Table II to estimate systematic uncertainties then for the volume–average base parameters, we have[11] $H_0 = 61.0\,\mathrm{km\ sec^{-1}\,Mpc^{-1}}$ (±1.3% stat) (±8% sys), and a present void volume fraction $f_{\mathrm{v}0} = 0.627$ (±2.33% stat) (±13% sys). This corresponds to a dressed matter density[12] $\Omega_{\mathrm{M}0} = 0.489$ (±3.3% stat) (±20% stat), which is consistent with the bounds on this parameter obtained from supernovae data using the SDSS-II sample [78], as shown in Fig. 8 of Ref. [6] .

Since the wall–geometry matching methods are better adapted to those aspects of the timescape model that do not relate directly to volume–average evolution, we use the $\mathrm{W}(k \neq 0)$ method – which has the best likelihood overall – to provide our best estimates on the parameters $\eta_{B\gamma}$ and n_{s}, and the $\mathrm{A}(\bar{H}_{\mathrm{dec}})$ method to estimate their systematic uncertainties. This gives $10^{10}\eta_{B\gamma} = 6.08$ (±1.5% stat) (±8.5% sys) and $n_{\mathrm{s}} = 0.96$ (±0.9% stat) (±4.3% sys). These best fit values are close to their ΛCDM counterparts [71], but the systematic uncertainties more fully reflect the limitations of our procedure.

With these parameters the timescape cosmology remains competitive with the ΛCDM cosmology, also when considering other cosmological tests, as summarized recently in Ref. [12]. However, since many best fit parameters in Table II are very close to ΛCDM values, this also means that parameter tensions may in some cases be similar. For example, a recent determination of the radial and angular baryon acoustic oscillation scales in the Lyman–α forest at a redshift $z = 2.34$ found a $2.5\,\sigma$ tension [79] with the ΛCDM parameters from Planck [71]. For the timescape model the values of $d_A(z)/r_{\mathrm{drag}}$ and $c/[H(z)r_{\mathrm{drag}}]$ are so close to the ΛCDM values at $z = 2.34$ [79] that it must also suffer tension of a similar magnitude. (However, one should add the caveat that the treatment of redshift space distortions may need to be revisited in non–FLRW models with backreaction [49].)

Our results are of course also limited by the fact that the late time ISW effect has not yet been computed for the timescape scenario, as it requires a from–first–principles reanalysis. This effect is important for the anisotropy spectrum at large angles, and we have therefore limited our analysis to large angle multipoles $\ell > 50$. If the timescape scenario is correct, then we might also expect a nonkinematic contribution to the CMB dipole below the scale of statistical homogeneity. Evidence

[11] In the case of the systematic uncertainties, the lower bound is what was actually obtained using the $\mathrm{W}(k = 0)$ and $\mathrm{W}(k \neq 0)$ matching procedures in Table II. However, since other matching procedures could be also envisioned, we use the bound obtained as a best estimate percentage systematic uncertainty.

[12] While this parameter is numerically closer to the FLRW value than the bare parameter is, since it does not obey a Friedmann–like equation it is not directly subject to the observational constraints that are placed on the parameter $\Omega_{\mathrm{M}0}$ of the standard cosmology. The two parameters cannot be equated.

for this was found in a recent model–independent analysis [29] of the variation of the Hubble expansion on $\lesssim 120\,h^{-1}$Mpc scales. This suggests that a detailed analysis of the large angle anisotropies, and of potential anomalies, requires not only a computation of the late time ISW effect in the timescape scenario, but also the impact that the subtraction of a nonkinematic dipole component would have on the map–making procedures in the CMB analysis.

To make more accurate predictions in the timescape scenario, it is of course necessary to eliminate the large systematic uncertainties that arise from the imprecise nature of the matched FLRW model procedures. This would require a huge computational effort. However, our results highlight the fact that important details of the acoustic peaks are strongly constrained by the ratio of baryonic to nonbaryonic matter in the primordial plasma, which can in principle differ in the timescape scenario. To treat this question rigorously we must address the effect of backreaction in the primordial plasma, and the manner in which the growth of structure is changed when the average evolution is very close to, but not exactly, a perturbative FLRW model. This question – which could change some of the conclusions of this paper – has not been studied, but is crucially important, not only for the timescape model but for all approaches to inhomogeneous cosmology with backreaction.

Acknowledgments

This work was supported by the Marsden Fund of the Royal Society of New Zealand. We have benefited from use of the publicly available computer codes [80] CLASS [55, 56], `CosmoMc` [59], `emcee` [62], `fastbbn` [64, 65], `HyRec` [68] and RECFAST [69, 70]. We thank Julien Lesgourgues for advice in implementing CLASS.

Appendix A: Additional relativistic species

We have also investigated the case when $N_{\rm eff}$ is left free to vary as an additional MCMC parameter, without elaborating what the extra radiation component represents. We do not aim to constrain neutrino masses, for example.

Varying $N_{\rm eff}$ affects the Boltzmann equations directly, and also the BBN helium abundance, $Y_{\rm p} = Y_{\rm p}(N_{\rm eff}, \eta_{B\gamma})$, which is passed to other parts of the code.

We find that the results with $N_{\rm eff}$ free to vary do not differ significantly from the case $N_{\rm eff} = 3.046$ of the base model. The results are shown in Table III for the canonical $\mathrm{A}(\bar{H}_{\rm dec})$ matching method. One reason for this investigation was to check whether the lithium anomaly problem could be alleviated at all by leaving $N_{\rm eff}$ free to deviate from 3.046. Deviations are possible if there are extra radiation components or a neutrino/antineutrino asymmetry, to list a couple of scenarios. This could be possible if BBN determination of $Y_{\rm p} = Y_{\rm p}(N_{\rm eff}, \eta_{B\gamma})$ forced $\eta_{B\gamma}$ towards lower values, $\eta_{B\gamma} \approx (5.1 \pm 0.5) \times 10^{-10}$, which resolve the lithium abundance anomaly [52, 53].

On the contrary we found preference for $N_{\rm eff} > 3.046$ and because $N_{\rm eff}$ is positively correlated with $\eta_{B\gamma}$ this leads to an even slightly larger $\eta_{B\gamma}$. This is accompanied with a preference for increased $f_{\rm v0}$ because $\eta_{B\gamma}$ is positively correlated with $f_{\rm v0}$ but negatively correlated with $\Omega_{\rm M0}$. (See Fig. 10.)

[1] D.L. Wiltshire, New J. Phys. **9**, 377 (2007).
[2] D.L. Wiltshire, Phys. Rev. Lett. **99**, 251101 (2007).
[3] D.L. Wiltshire, Phys. Rev. **D 80**, 123512 (2009).
[4] D.L. Wiltshire, Phys. Rev. **D 78**, 084032 (2008).
[5] B.M. Leith, S.C.C. Ng, and D.L. Wiltshire, Astrophys. J. **672**, L91 (2008).
[6] P.R. Smale and D.L. Wiltshire, Mon. Not. R. Astr. Soc. **413**, 367 (2011).
[7] P.R. Smale, Mon. Not. R. Astr. Soc. **418**, 2779 (2011).
[8] J.A.G. Duley, M.A. Nazer, and D.L. Wiltshire, Class. Quantum Grav. **30**, 175006 (2013).
[9] D.W. Hogg, D.J. Eisenstein, M.R. Blanton, N.A. Bahcall, J. Brinkmann, J.E. Gunn, and D.P. Schneider, Astrophys. J. **624**, 54 (2005).
[10] F. Sylos Labini, N.L. Vasilyev, L. Pietronero, and Y.V. Baryshev, Europhys. Lett. **86**, 49001 (2009).
[11] M. Scrimgeour, T. Davis, C. Blake *et al*, Mon. Not. R. Astr. Soc. **425**, 116 (2012).
[12] D.L. Wiltshire, in S.E. Perez Bergliaffa and M. Novello (eds), *Proceedings of the XVth Brazilian School of Cosmology and Gravitation*, (Cambridge Scientific Publishers, Cambridge, 2014); `arXiv:1311.3787`.
[13] F. Hoyle and M.S. Vogeley, Astrophys. J. **566**, 641 (2002).
[14] F. Hoyle and M.S. Vogeley, Astrophys. J. **607**, 751 (2004).
[15] D.C. Pan, M.S. Vogeley, F. Hoyle, Y.Y. Choi, and C. Park, Mon. Not. R. Astr. Soc. **421**, 926 (2012).
[16] L.J. Liivamägi, E. Tempel and E. Saar, Astron. Astrophys. **539**, A80 (2012).
[17] S. Nadathur and S. Hotchkiss, Mon. Not. R. Astr. Soc. **440**, 1248 (2014).
[18] A.V. Tikhonov and I.D. Karachentsev, Astrophys. J. **653**, 969 (2006).
[19] G.F.R. Ellis, in B. Bertotti, F. de Felice, and A. Pascolini (eds), *General Relativity and Gravitation*, (Reidel, Dordrecht, 1984) pp. 215–288.
[20] G.F.R. Ellis and W. Stoeger, Class. Quantum Grav. **4**, 1697 (1987).
[21] D.L. Wiltshire, Class. Quantum Grav. **28**, 164006 (2011).
[22] G. Lemaître, Ann. Soc. Sci. Bruxelles **A 53**, 51 (1933) [English translation: Gen. Relativ. Grav. **29**, 641 (1997)].

TABLE III: The analysis of Table II is repeated with $N_{\rm eff}$ free to vary.

Matching type		A($\bar{H}_{\rm dec}$)		W($k=0$)		W($k\neq 0$)
Parameter	Best fit	Mean (68% limits)	Best fit	Mean (68% limits)	Best fit	Mean (68% limits)
$f_{\rm v0}$	0.637	0.630 ± 0.014	0.551	$0.549^{+0.021}_{-0.018}$	0.560	$0.562^{+0.019}_{-0.018}$
H_0	62.263	$61.451^{+1.047}_{-1.034}$	56.533	$56.398^{+2.162}_{-2.110}$	57.157	$57.419^{+2.395}_{-1.831}$
$N_{\rm eff}$	3.243	$3.110^{+0.098}_{-0.110}$	3.062	$3.060^{+0.387}_{-0.371}$	3.129	$3.168^{+0.404}_{-0.348}$
$10^{10}\eta_{\rm B\gamma}$	6.533	$6.518^{+0.108}_{-0.109}$	6.066	6.047 ± 0.109	6.124	$6.112^{+0.111}_{-0.108}$
$n_{\rm s}$	1.001	$0.996^{+0.011}_{-0.012}$	0.959	$0.956^{+0.020}_{-0.018}$	0.962	$0.965^{+0.020}_{-0.016}$
$\bar{H}_0$	52.425	$51.942^{+0.513}_{-0.512}$	50.001	$49.918^{+1.487}_{-1.426}$	50.317	$50.466^{+1.598}_{-1.253}$
$\bar{T}_0$	2.066	2.072 ± 0.011	2.136	$2.138^{+0.015}_{-0.018}$	2.129	$2.127^{+0.014}_{-0.017}$
t_0	16.398	$16.510^{+0.117}_{-0.116}$	16.633	$16.657^{+0.369}_{-0.425}$	16.584	$16.560^{+0.339}_{-0.430}$
$\bar{\gamma}_0$	1.319	1.316 ± 0.007	1.276	$1.275^{+0.011}_{-0.009}$	1.280	1.282 ± 0.009
$Y_{\rm p}$	0.2507	$0.2489^{+0.00142}_{-0.00152}$	0.248	$0.247^{+0.006}_{-0.005}$	0.249	$0.249^{+0.006}_{-0.004}$
$\bar{\Omega}_{\rm B0}$	0.038	0.039 ± 0.001	0.043	$0.043^{+0.002}_{-0.003}$	0.042	$0.042^{+0.002}_{-0.003}$
$\bar{\Omega}_{\rm C0}$	0.170	$0.175^{+0.009}_{-0.010}$	0.233	$0.234^{+0.012}_{-0.016}$	0.226	$0.225^{+0.012}_{-0.014}$
$\bar{\Omega}_{\rm M0}$	0.208	0.213 ± 0.010	0.275	$0.277^{+0.014}_{-0.018}$	0.268	$0.266^{+0.014}_{-0.017}$
$\bar{\Omega}_{\rm k0}$	0.825	$0.820^{+0.010}_{-0.009}$	0.763	$0.761^{+0.017}_{-0.013}$	0.769	$0.771^{+0.016}_{-0.013}$
$\bar{\Omega}_{\mathcal{Q}0}$	-0.033	-0.034 ± 0.001	-0.038	-0.038 ± 0.001	-0.038	-0.038 ± 0.001
$\bar{z}_{\rm dec}$	1434.924	$1431.143^{+7.060}_{-6.898}$	1391.235	$1390.203^{+11.336}_{-9.740}$	1395.612	$1396.985^{+10.853}_{-9.437}$
$\bar{z}_{\rm drag}$	1402.388	$1398.465^{+8.044}_{-7.965}$	1352.757	$1351.460^{+12.537}_{-10.983}$	1357.923	$1359.065^{+12.386}_{-10.305}$
$\bar{D}_s(\bar{z}_{\rm dec})$	0.134	0.134 ± 0.001	0.132	0.132 ± 0.003	0.132	0.132 ± 0.003
$\bar{D}_s(\bar{z}_{\rm drag})$	0.139	0.140 ± 0.001	0.139	0.139 ± 0.003	0.138	$0.138^{+0.003}_{-0.004}$
$\tau_{\rm w0}$	13.606	13.732 ± 0.144	14.228	$14.260^{+0.369}_{-0.449}$	14.145	$14.114^{+0.327}_{-0.448}$
$\Omega_{\rm B0}$	0.087	0.088 ± 0.001	0.089	$0.089^{+0.003}_{-0.005}$	0.088	$0.088^{+0.003}_{-0.004}$
$\Omega_{\rm C0}$	0.391	0.397 ± 0.015	0.483	$0.485^{+0.016}_{-0.019}$	0.474	$0.472^{+0.017}_{-0.018}$
$\Omega_{\rm M0}$	0.478	$0.486^{+0.015}_{-0.016}$	0.572	$0.574^{+0.019}_{-0.022}$	0.563	$0.560^{+0.019}_{-0.020}$
$z_{\rm dec}$	1087.557	$1087.479^{+0.484}_{-0.499}$	1090.001	$1090.064^{+0.530}_{-0.535}$	1089.781	$1089.869^{+0.563}_{-0.551}$
$z_{\rm drag}$	1062.892	$1062.638^{+0.831}_{-0.839}$	1059.849	$1059.672^{+1.401}_{-1.412}$	1060.345	$1060.272^{+1.520}_{-1.263}$
$100\,\theta_{\rm dec}$	1.047	1.047 ± 0.001	1.041	1.041 ± 0.001	1.041	1.041 ± 0.001
$100\,\theta_{\rm drag}$	1.063	1.064 ± 0.001	1.061	1.061 ± 0.002	1.060	$1.060^{+0.001}_{-0.002}$
$d_{\rm A}$	12.774	12.840 ± 0.101	12.706	$12.724^{+0.279}_{-0.283}$	12.686	$12.673^{+0.249}_{-0.310}$
$d_{\rm A,drag}$	13.065	$13.136^{+0.097}_{-0.096}$	13.062	$13.083^{+0.296}_{-0.304}$	13.033	$13.022^{+0.264}_{-0.331}$

[23] R.C. Tolman, Proc. Nat. Acad. Sci. **20**, 169 (1934).
[24] H. Bondi, Mon. Not. R. Astr. Soc. **107**, 410 (1947).
[25] P. Szekeres, Commun. Math. Phys. **41**, 55 (1975).
[26] T. Buchert, Gen. Relativ. Grav. **40**, 467 (2008).
[27] C. Clarkson, G.F.R. Ellis, J. Larena, and O. Umeh, *Rept. Prog. Phys.* **74**, 112901 (2011).
[28] R.J. van den Hoogen, in T. Damour, R. T. Jantzen, and R. Ruffini (eds), *Proceedings of the 12th Marcel Grossmann Meeting on General Relativity*, (World Scientific, Singapore, 2012) pp. 578-589.
[29] D.L. Wiltshire, P.R. Smale, T. Mattsson, and R. Watkins, Phys. Rev. **D 88**, 083529 (2013).
[30] T. Buchert, Gen. Relativ. Grav. **32**, 105 (2000).
[31] T. Buchert, Gen. Relativ. Grav. **33**, 1381 (2001).
[32] W. Hu and N. Sugiyama, Astrophys. J. **444**, 489 (1995).
[33] S. Weinberg, *Cosmology*, (Oxford University Press, 2008).
[34] S. Dodelson, *Modern Cosmology*, (Academic Press, Amsterdam, 2003).
[35] V. Mukhanov, *Physical Foundations of Cosmology*, (Cambridge University Press, 2005).
[36] J. Lesgourgues, G. Mangano, G. Miele, and S. Pas-

tor, *Neutrino Cosmology*, (Cambridge University Press, 2013).
[37] K. Bolejko and J.S.B. Wyithe, J. Cosmol. Astropart. Phys. 02 (2009) 020.
[38] T. Biswas, A. Notari, and W. Valkenburg, J. Cosmol. Astropart. Phys. 11 (2010) 030.
[39] C. Clarkson and M. Regis, J. Cosmol. Astropart. Phys. 02 (2011) 013.
[40] A. Moss, J.P. Zibin, and D. Scott, Phys. Rev. **D 83**, 103515 (2011).
[41] S. Nadathur and S. Sarkar, Phys. Rev. **D 83**, 063506 (2011).
[42] M. Vonlanthen, S. Räsänen, and R. Durrer, J. Cosmol. Astropart. Phys. 08 (2010) 023.
[43] J.P. Zibin, A. Moss, and D. Scott, Phys. Rev. **D 76**, 123010 (2007).
[44] T. Clifton, P.G. Ferreira, and J. Zuntz, J. Cosmol. Astropart. Phys. 07 (2009) 029.
[45] T. Buchert and M. Carfora, Class. Quantum Grav. **19**, 6109 (2002).
[46] T. Buchert and M. Carfora, Phys. Rev. Lett. **90**, 031101 (2003).
[47] B.F. Roukema, J.J. Ostrowski, and T. Buchert, J. Cosmol. Astropart. Phys. 10 (2013) 043.
[48] M. Lavinto, S. Räsänen, and S.J. Szybka, J. Cosmol. Astropart. Phys. 12 (2013) 051.
[49] B.F. Roukema, T. Buchert, J.J. Ostrowski, and M.J. France, Mon. Not. R. Astr. Soc. **448**, 1660 (2015).
[50] C. Clarkson, B. Bassett, and T.H.C. Lu, Phys. Rev. Lett. **101**, 011301 (2008).
[51] D. Sapone, E. Majerotto, and S. Nesseris, Phys. Rev. **D 90**, 023012 (2014).
[52] G. Steigman, Int. J. Mod. Phys. **E 15**, 1 (2006).
[53] R.H. Cyburt, B.D. Fields, and K.A. Olive, J. Cosmol. Astropart. Phys. 11 (2008) 012.
[54] A. Lewis, A. Challinor, and A. Lasenby, Astrophys. J. **538**, 473 (2000).
[55] J. Lesgourgues, `arXiv:1104.2932`.
[56] D. Blas, J. Lesgourgues, and T. Tram, J. Cosmol. Astropart. Phys. 07 (2011) 034.
[57] P.A.R. Ade *et al* [Planck collaboration], Astron. Astrophys. **571**, A15 (2014).
[58] N. Metropolis, A.W. Rosenbluth, M.N. Rosenbluth, A.H. Teller, and E. Teller, J. Chem. Phys. **21**, 1087 (1953).
[59] A. Lewis and S. Bridle, Phys. Rev. **D 66**, 103511 (2002).
[60] R. Allison and J. Dunkley, Mon. Not. R. Astr. Soc. **437**, 3918 (2014).
[61] J. Goodman and J. Weare, Commun. Appl. Math. Comput. Sci. **5**, 65 (2010).
[62] D. Foreman-Mackey, D.W. Hogg, D. Lang, and J. Goodman, Publ. Astron. Soc. Pac. **125**, 306 (2013).
[63] http://www-thphys.physics.ox.ac.uk/users/SubirSarkar/bbn/fastbbn.f
[64] G. Fiorentini, E. Lisi, S. Sarkar, and F.L. Villante, Phys. Rev. **D 58**, 063506 (1998).
[65] E. Lisi, S. Sarkar, and F.L. Villante, Phys. Rev. **D 59**, 123520 (1999).
[66] C.-P. Ma and E. Bertschinger, Astrophys. J. **455**, 7 (1995).
[67] P.J.E. Peebles, Astrophys. J. **153**, 1 (1968).
[68] Y. Ali-Haimoud and C.M. Hirata, Phys. Rev. **D 83**, 043513 (2011)
[69] S. Seager, D.D. Sasselov, and D. Scott, Astrophys. J. **523**, L1 (1999).
[70] D. Scott and A. Moss, Mon. Not. R. Astr. Soc. **397**, 445 (2009).
[71] P.A.R. Ade *et al* [Planck collaboration], Astron. Astrophys. **571**, A16 (2014).
[72] D.J. Fixsen, Astrophys. J. **707**, 916 (2009).
[73] J. Beringer *et al* [Particle Data Group Collaboration], Phys. Rev. **D 86**, 010001 (2012).
[74] G. Mangano, G. Miele, S. Pastor, T. Pisanti, and D.P. Serpico, Nucl. Phys. **B 729**, 221 (2005).
[75] A. Gelman and D. Rubin, Statist. Sci. **7**, 457 (1992).
[76] G. Hinshaw *et al* [WMAP Collaboration], Astrophys. J. Suppl. **208**, 19 (2013).
[77] http://pla.esac.esa.int/pla/
[78] R. Kessler, A. Becker, D. Cinabro, *et al*, 2009, Astrophys. J. Suppl. **185**, 32.
[79] T. Delubac *et al* [BOSS Collaboration], Astron. Astrophys. **574**, A59 (2015).
[80] The programs are freely distributed with unstated licences, with the exception of `emcee` which is distributed under the MIT licence, http://opensource.org/licenses/MIT.